

# Experimental Investigation of Buckling Restrained Braces for Bridge Bidirectional Ductile End Diaphragms

Xiaone Wei<sup>1</sup> and Michel Bruneau, F.ASCE<sup>2</sup>

**Abstract:** Quasi-static experiments were conducted to subject buckling restrained braces (BRBs) to a regime of relative end displacements demands to investigate if the BRBs' end connections could be able to sustain the required displacement demands when installed in bidirectional ductile end diaphragm systems (EDS). The loading protocols included the bidirectional displacement histories to be applied to the specimens for the cyclic inelastic test and the uniaxial displacement histories for the low-cycle fatigue test caused by temperature changes. Two types of BRBs with flat end plates and unidirectional pinholes, namely BRB-1 and BRB-2, were designed and tested. Four specimens of each type of BRB were tested under combinations of different displacement protocols, and the resulting BRBs' hysteretic behaviors were studied and compared. All the BRB specimens tested developed cumulative inelastic deformations of more than 200 times the BRB's axial yield displacement. The specimens were able to sustain multiple years of severe temperature cycles in addition to meeting the seismic qualification test criterion. Ultimately, as expected, all BRBs failed in tension after extensive cycles of inelastic deformations. No undesirable end-plate failure or instability was observed. A recommended design procedure for the EDS with BRBs in both straight and skew bridges was developed based on these experimental results. DOI: [10.1061/\(ASCE\)ST.1943-541X.0002042](https://doi.org/10.1061/(ASCE)ST.1943-541X.0002042). © 2018 American Society of Civil Engineers.

**Author keywords:** Bidirectional ductile end diaphragm; Buckling restrained braces; Bidirectional test; Temperature-related displacements; Design procedure.

## Introduction

The concept of a bidirectional ductile end diaphragm system (EDS) was first proposed by Celik and Bruneau (2011), in which buckling restrained braces (BRBs) were studied to be implemented in the superstructure of a slab-on-girder steel bridge to improve its seismic performance. In the EDS schemes, two pairs of BRBs are located at each end of a span, in a configuration that coincides with the skew and longitudinal directions of the bridge as shown in Fig. 1. The deck is assumed to be supported on bidirectional sliding bearings or other bearings with negligible strength to horizontal deformations at the abutment. For both EDS configurations, closed-form equations were given to show the relationship among stiffness, yield strength, yield displacement, and hysteretic energy dissipation as a function of a given design ductility level. Static pushover analyses were performed to study how the change of certain parameters could affect the systems' behaviors.

Wei and Bruneau (2017) investigated the dynamic inelastic response of these two ductile EDS schemes when subjected to actual earthquake excitations by conducting parametric nonlinear time-history analyses of bridge models with various skewness, EDS configurations, and ground motion intensities, and provided equations to obtain seismic end-displacement demands of the BRBs. In both EDS schemes, BRBs spanning across the bridge expansion joints [i.e., between the abutment and bridge deck, as schematically

shown in Fig. 2(a)] will be subjected to the cyclic bidirectional displacement demands because of an earthquake, as well as axial strains induced in the BRBs as a consequence of thermal movements of the bridge during regular service. The design of BRBs in the EDS has to consider both sources of displacements demands, which can produce failure of the BRB's steel core plate and end plates.

BRB is a type of hysteretic device that has its steel core plate encased. With the global buckling prevented, BRBs have been proven able to sustain a large significant number of cycles at large ductility demands and develop stable hysteresis when subjected to in-plane cyclic loading (Clark et al. 2000; Black et al. 2002; Lopez et al. 2002; Aiken et al. 2002; Merritt et al. 2003a, b; Usami et al. 2003; Tsai et al. 2003; Lopez and Sabelli 2004; Uang et al. 2004; Tremblay et al. 2006; Romero et al. 2007; Fahnestock et al. 2007; Bruneau et al. 2011). However, the BRB's design axial strength in the core plate can only be reached when its end connections are designed to avoid out-of-plane instability issues. For BRB steel frame (BRBF) systems tested in the past, BRBs are normally designed to connect to the framing elements (beams and columns) using gusset plates. In a few BRBF tested unidirectionally (Aiken et al. 2002; Roeder et al. 2006; Tremblay et al. 2006, Tsai et al. 2008; Palmer et al. 2013), the kind of out-of-plane instability of the BRBs has been observed. The gusset plates in some large-scale tests of BRB planar subassemblies and three-dimensional BRBF systems have exhibited poor performance at story drifts between 2 and 2.5% (Fahnestock et al. 2007).

Palmer et al. (2013) tested a full three-dimensional 2-story frame, with one-bay BRBFs in each direction. Although the BRB's core plates failed at 3.6 and 4.2% story drift, significant inelastic deformations and damage were reported in the framing member of the system and gusset plates, which exhibited gusset-plate weld tearing and buckling at 2% story drift. The ability of the BRBs in the BRBF to resist bidirectional loading relies on the bending

<sup>1</sup>Civil Associate, Michael Baker International, 200 W Adams St., Chicago, IL 60606 (corresponding author). E-mail: [xiaonewe@buffalo.edu](mailto:xiaonewe@buffalo.edu)

<sup>2</sup>Professor, Dept. of Civil, Structural, and Environmental Engineering, Univ. at Buffalo, Buffalo, NY 14260. E-mail: [bruneau@buffalo.edu](mailto:bruneau@buffalo.edu)

Note. This manuscript was submitted on July 10, 2017; approved on November 16, 2017; published online on March 27, 2018. Discussion period open until August 27, 2018; separate discussions must be submitted for individual papers. This paper is part of the *Journal of Structural Engineering*, © ASCE, ISSN 0733-9445.

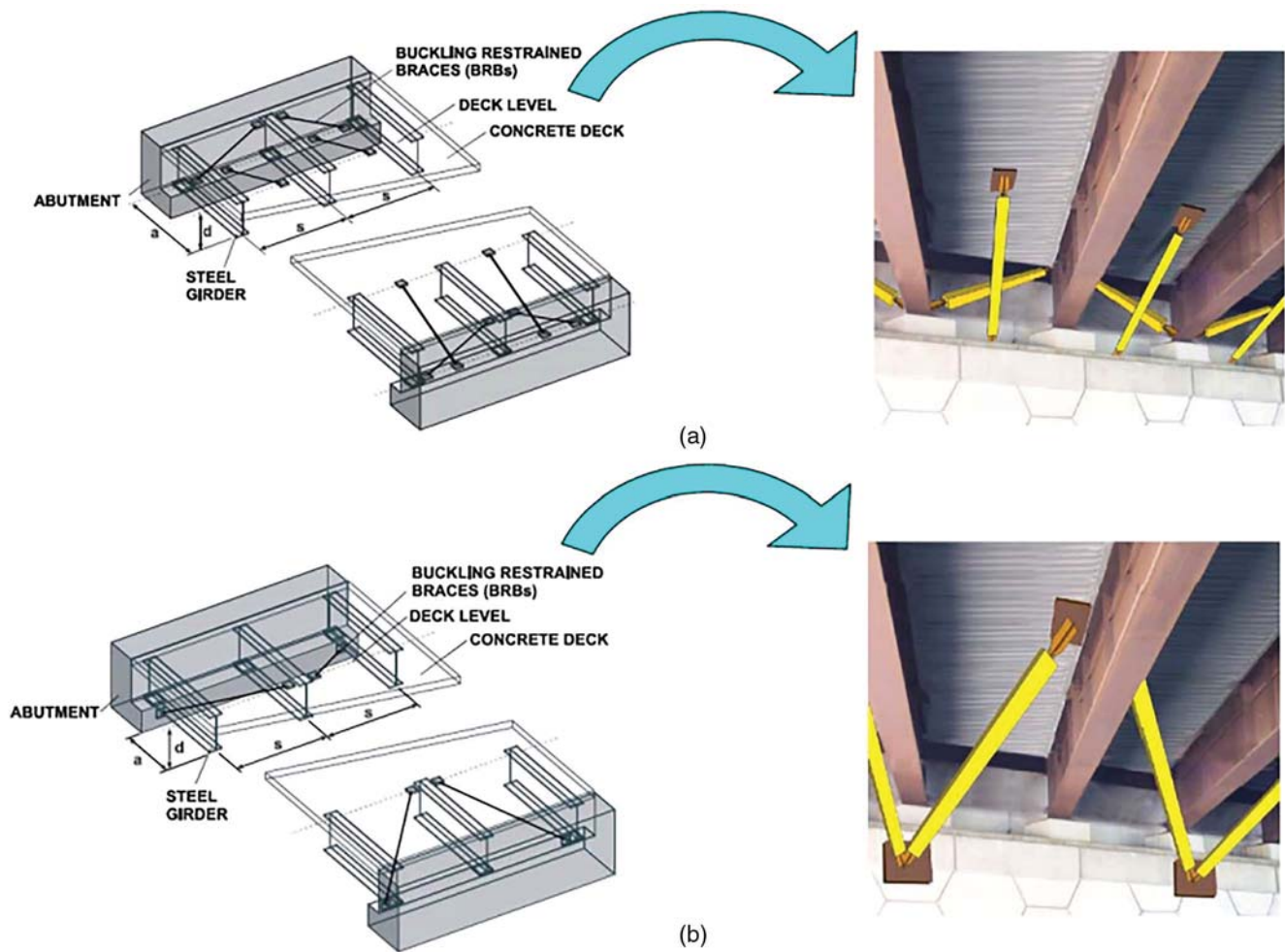


Fig. 1. Two types of bridge ductile end diaphragm systems with BRBs (adapted from Celik and Bruneau 2007): (a) EDS-1; (b) EDS-2

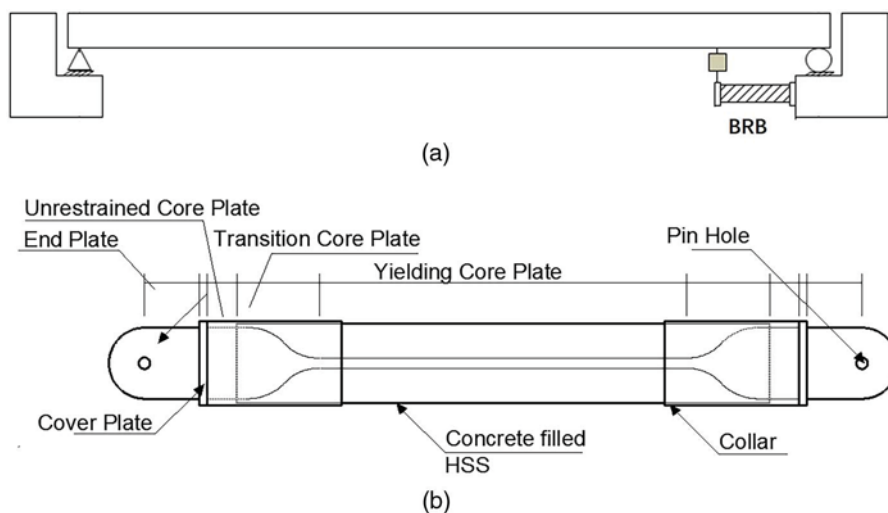


Fig. 2. (a) Bridge model with BRB connecting the bridge abutment and girder; (b) side view of a typical BRB specimen

flexibility of the gusset plates to which the BRBs are connected. The BRB in the EDS has to be designed for bidirectional displacement demands, which may be larger than 2%. Therefore, the out-of-plane displacement capability of the connection has to be investigated through tests.

Tsai and Hsiao (2008) improved the seismic performance of the BRBF by addressing the out-of-plane buckling of the gusset plate that connected a BRB to a column. Edge stiffeners were added to the gusset plate, and the effective length factor,  $K$ , used to design the gusset plate, was suggested as 0.65 and 2 for cases with and

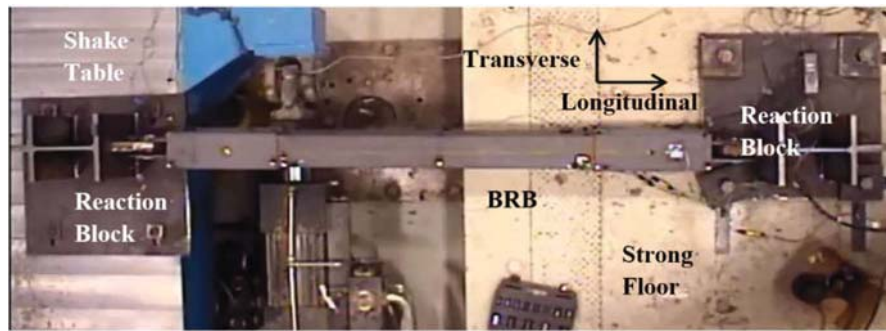


Fig. 3. Quasi-static test setup with BRB

without edge stiffeners, respectively. The Architectural Institute of Japan (AIJ 2009) contains two models considered for preventing the global instability of bolted-end BRBs. The rationale for these two models was best explained by Koetaka et al. (2008) and Takeuchi et al. (2014), who investigated the stability of BRB per these two concepts, respectively. Differential equations for the compression member were formulated, and the boundary conditions were used to obtain the buckling strength of the BRB/connection system, which consists of the connection and restrained zone.

Because the BRB application in bidirectional ductile EDS requires even larger out-of-plane displacement capacity than any BRB ever tested, in order to develop and validate the bidirectional ductile EDS concept to a point that is ready for implementation, this paper investigates two types of BRB end-connection details to improve the BRB's bidirectional displacement capacity, especially in the transverse direction (i.e., out-of-plane). Quasi-static tests were performed on these two types of BRBs (four specimens of each type) by subjecting them to different scenarios of individual or sequential displacement protocols representative of the bidirectional and axial temperature-induced displacement results predicted from parametric analytical studies [presented by Wei and Bruneau (2017)]. This paper presents the ultimate inelastic cyclic performance of the BRB specimens under these different displacement protocols, summarizes and compares the cumulative inelastic deformations and fatigue damage of each tested BRB, and proposes a recommended design procedure for bidirectional EDS with BRBs.

## BRB Specimens, Test Setup, and Instrumentation

### Test Setup and BRB Specimens

Two types of BRBs with pin end connections, named BRB-1 and BRB-2, were designed and tested. They were manufactured and supplied by Star Seismic (Park City, Utah). Fig. 2(b) shows the side view of a typical BRB specimen. Both BRBs have two flat end plates with holes at their end, designed such that the BRB could be pin-connected to gusset plates in the reaction blocks located on the strong floor or the shake table in the test setup shown in Fig. 3. One end of the BRB was connected to a reaction block, itself tied down to holes in the strong floor. The other end was connected to the shake table, which was then used to apply horizontal bidirectional end-displacement demands to the BRB. The BRB's core plate was encased in a concrete-filled steel hollow structural section (HSS). The end collar at each end of the BRB prevents instability of the core plate when it extends outside of the concrete restraining material.

The reaction blocks in Fig. 3 were made of a W-shaped steel section welded to a base plate, and gusset plates were welded to

the W-shape and base plate. The gusset plates were designed to remain elastic when resisting the maximum tensile and compressive forces developed by the BRB without yielding or buckling. Gusset Plate 1 and Gusset Plate 2 were used to connect BRB-1 and BRB-2, as shown in Fig. 4. A bolt was used to connect the Gusset Plate 1 to BRB-1 at each end. A spherical bearing allowing multidirectional movement was inserted to fit in the hole in the Gusset Plate 2 to connect to BRB-2 at each end using a pin.

### Seismic Displacement Demands

The BRBs' end connections need to sustain the required displacement demands when installed in the EDS, especially the transverse displacement that could cause flexural yielding of the BRB's end plates beyond the target design displacement. The BRB's end plates were sized such that the shake table's maximum displacement capacity could be used to test the BRB and examine the BRB's connection behavior beyond yielding and investigate its failure mode.

A straight (nonskew) simply supported single-span steel slab-on-girder bridge was considered as the prototype bridge in this study. This bridge has girders spaced at 1.829 m (72 in.) center to center. The height of the girder is 1.829 m (72 in.). The deck is assumed to be supported on bidirectional sliding bearings or other bearings with negligible strength to horizontal deformations at the abutment. The bridge length is assumed to be 30.48 m (100 ft). The weight of the bridge is  $8.9 \times 10^6$  N (2,000 kips). The corresponding simplified bridge model with a rigid bridge deck is shown in Fig. 5. At the ends of the span, the thicker solid lines in the enlarged view represent the structural elements used to model the EDS at both ends of the bridge, whereas the gray line are reference lines. The lines with symbols represent the BRBs in the longitudinal and transverse direction, and they can be visualized as the shaded structural members in Fig. 1. The flexibility of the girder and slab was neglected, as well as the stiffness contribution from the bearing web stiffeners.

At the time of analyzing this bridge model, the details of the BRB specimens to be tested were unknown. To size the BRB specimen and assess the design displacements to consider in the test, nonlinear time history analyses were performed for the nonskew bridge model having the target BRB (circled in Fig. 5) as the longitudinal BRB of 2.54 m (100 in.) in length and assumed yield strength of  $1.78 \times 10^5$  (40 kips). This longitudinal BRB, i.e., generic BRB, was assumed to have an inclination angle of  $45^\circ$  from the bridge deck. The yield length ratio factor of the BRB's core plate was assumed to be 0.5. The material of the steel core was assumed to be A36 with expected yield strength of 289.6 MPa (42 ksi). The cross-sectional area of the BRB's core plate was designed as  $612.9 \text{ mm}^2$  ( $0.95 \text{ in.}^2$ ). Without the BRB specimens'

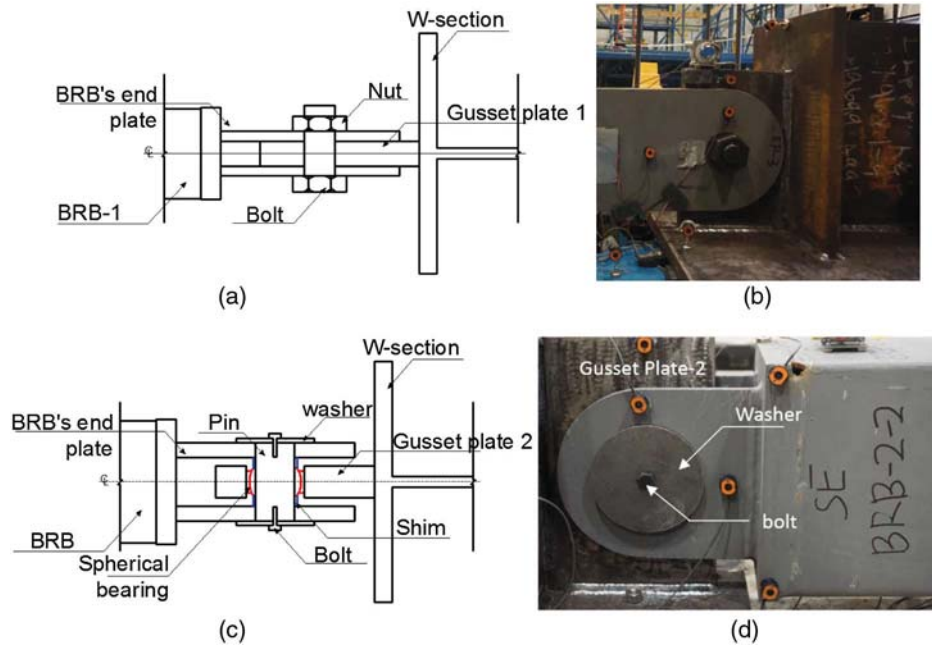


**Fig. 4.** (a) Section cut of the BRB-1 with Gusset Plate 1 connection; (b) side view of BRB-1 with reaction block connection; (c) section cut of BRB-2 with Gusset Plate 2 connection; (d) side-view of BRB-2 with reaction block connection

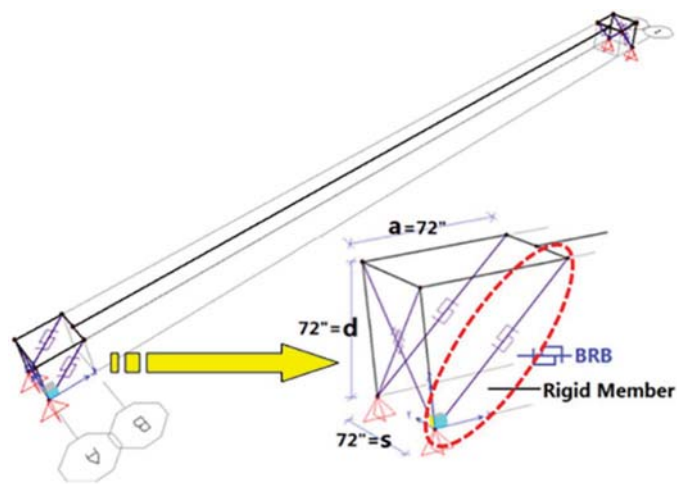


**Fig. 5.** Bridge with BRBs in the EDS and enlarged view at the end

details, the BRB's axial yield displacement,  $D_{by}$ , was calculated only for the deformation of the yielding core plate length, which is 1.88 mm (0.074 in.). This approximate calculation of the yield deformation has been used by Lopez and Sabelli (2004). When the plates outside of the core were significantly larger and their length significantly smaller, it is rational to take them as rigid for sake of preliminary stiffness calculations.

Orthogonal components of the ground motion records were inputted in the global longitudinal and transverse directions of the bridge model when performing the nonlinear time-history analyses to investigate inelastic displacement demands of the BRBs in the EDS. The behaviors of the EDS in the two orthogonal directions are uncoupled in the nonskew bridge, and the system can be detailed to behave in a bilinear manner. The 44 ground motions specified in FEMA-P695 (FEMA 2009) were used to perform the nonlinear time-history analyses. Although this set of 44 ground motions

recommended by FEMA-P695 was developed for studies on building structures, using them was adequate here because it provided a broad variability of ground motions in order to generate the displacement demands. The EDS displacement limits in both directions can translate into maximum global ductility demand,  $\mu$ , themselves related to yielding displacement of the BRB in the EDS. The ground motions were scaled at each ductility level, and detailed information on scaling of the ground motions can be found in Wei and Bruneau (2017). Maximum transverse displacements of the bridge diaphragm model were obtained from 44 time-history analyses using the 22 pairs of ground motions. Because the bidirectional displacement protocols were mainly intended to test the BRB's transverse displacement capacity, target ductilities up to 11 were considered in order to explore greater possible transverse displacement demands. The target ductility of 9 resulted in the largest transverse displacement of 40.69 mm (1.602 in.) among these ductility demands, with a corresponding BRB axial displacement demand of 16.41 mm (0.646 in.).

Both types of the actual BRBs manufactured were expected to have slight differences in yield strength, cross-sectional area, and yielding core length from the generic BRB considered in the aforementioned model. To gauge the difference between displacement demands predicted earlier for the generic BRB and those that would occur with the actual BRBs installed in the prototype bridge, the model was reanalyzed for the same 22 pairs of ground motions scaled to target ductility of 9. For this actual BRB case, the resulted displacement demands were roughly 37 and 10% larger than using generic BRB in the longitudinal and transverse direction, respectively. Because it was time-consuming to perform the time-history analyses with 44 ground motions for the changed bridge model with different BRB properties, and because the tight scheduled window for testing in the lab could not allow such delay while waiting for the results of these analyses, the BRB-2 specimens, tested first, were subjected to the protocol considering the original displacements displacement values. However, the analyses were completed prior to the testing of the BRB-1 specimens, and changes were made to adjust the testing protocols for BRB-1 specimens.

## Design of BRB Specimens

The end plates of BRB-1 were designed to bend laterally to accommodate the required transverse displacement without developing instability. For BRB-1, the end plates were designed as beam-columns with a  $K$  factor of 2 to remain elastic under the maximum axial force that the BRB can develop by avoiding yielding in tension and buckling in compression. Its transverse yield displacement is obtained when the end plate reaches its flexural yield strength at the bottom of the cantilevering end plate under the BRB's maximum axial force. This transverse yield displacement should be larger than the target transverse displacement demand, making sure that BRB's end connection would not yield in flexure at design displacement. The end plates of BRB-2 were connected to a spherical bearing, itself kept in place in a predrilled hole in the gusset plates. Each spherical bearing works as a bidirectional hinge. The maximum transverse displacement that BRB-2 can sustain depends on the design of the spherical bearing in the reaction block.

The total pin-to-pin length of the BRB specimen is 2.54 m (100 in.), and the yielding core plate has a cross-section area of 645.2 mm<sup>2</sup> (1.0 in.<sup>2</sup>). The yielding core material was specified as A36 steel with expected yield strength of 317.2 MPa (46 ksi). BRB-1 has a yielding core length of 1.181 m (46.5 in.), whereas BRB-2's yielding core length is 1.275 m (50.2 in.) (resulting in a yield length ratio of 0.46 and 0.5 for BRB-1 and BRB-2, respectively). The distance between the pin hole and the point where the end plates are connected to the cover plate is 29.21 cm (15 in.) and 12.7 cm (5 in.) for BRB-1 and BRB-2, respectively. The BRB's core plate length is composed of three parts as shown in Fig. 2, which are the yielding core length,  $L_{ys}$ , transition core length,  $L_{ts}$ , and unrestrained core length,  $L_{us}$ . The calculated BRB's yield displacement,  $\Delta_{by}$ , from the sum of the respective deformation of each of these three parts, is 2.72 mm (0.107 in.) and 2.06 mm (0.081 in.) for BRB-1 and BRB-2, respectively.

## Instrumentation

A BRB's axial deformation was measured in three different ways in the tests, by using string potentiometer (SP), linear potentiometer (LP), and light-emitting diodes (LEDs) in the Krypton dynamic measurement machine system (Nikon Metrology NV, Belgium). LPs were installed at each BRB end to measure the displacement between the collar and HSS sleeve of the BRB. They were positioned at the top middle of the BRB as shown in Fig. 6(a). The sum

of the measured deformations from the two LPs is related to elongation of the BRB yielding core (directly measured by the SP), assuming no rotation of the collars. To capture the three-dimensional (3D) displacements of different parts in the BRB, the Krypton system tracked movement of 32 LEDs attached to the BRBs and reaction blocks. The layout of the LEDs used is shown in Fig. 6(b). Data from the SPs and LPs provided real-time display of the BRB's deformations during the tests, whereas movements of the LEDs captured by the Krypton camera (while providing more accurate measurement of displacements) required postprocessing of the data after completion of the test. However, Krypton data allowed calculating the relative rotation between the collar and HSS, rotation and lateral displacement of the BRB end plates, and slippage of the pins/bolts in the holes at each end, among many things.

Data output from the shake table included the forces applied in the table's longitudinal and transverse directions (where the longitudinal direction is defined by the axis of the BRB in its original position), and corresponding displacements. The BRB-1 specimens were also instrumented by strain gauges located on the end plates and collar to monitor if yielding occurred there; detailed information can be found in Wei and Bruneau (2015, 2016).

## BRB Test Protocols

Given that the target BRB in Fig. 5 is installed spanning across the bridge's expansion joint, axial strains in the BRB can be induced as a consequence of thermal movements of the bridge during regular service, or by an earthquake when the BRB is subjected to cyclic bidirectional displacement demands. The loading protocols developed here have considered both of these sources, which can produce inelastic deformations that can accumulate to produce low-cycle fatigue of the BRB's core plate.

## Bidirectional Qualification Test Protocol

AISC 341-10 (AISC 2010) specifies the standard test protocol developed for BRBs (tested alone and in subassemblies) principally subjected to axial displacements. The test protocol includes two cycles of loading at the deformations corresponding to  $1.0D_{by}$ ,  $0.5D_{bmL}$ ,  $1.0D_{bmL}$ ,  $1.5D_{bmL}$ , and  $2.0D_{bmL}$ , respectively, followed by additional cycles of loading at the deformation corresponding to  $1.5D_{bmL}$ , in which  $D_{by}$  and  $D_{bmL}$  are the first significant yield displacement and displacement corresponding to design story drift,

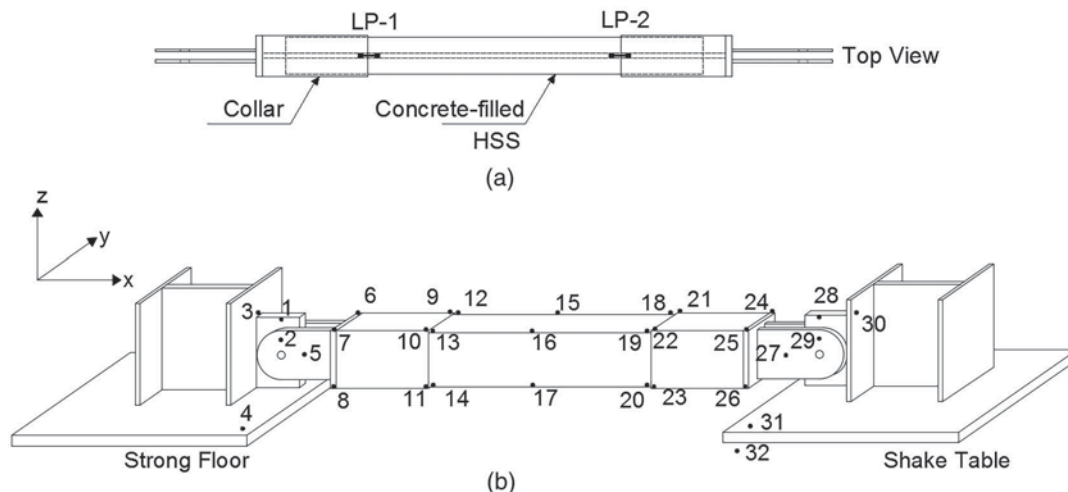
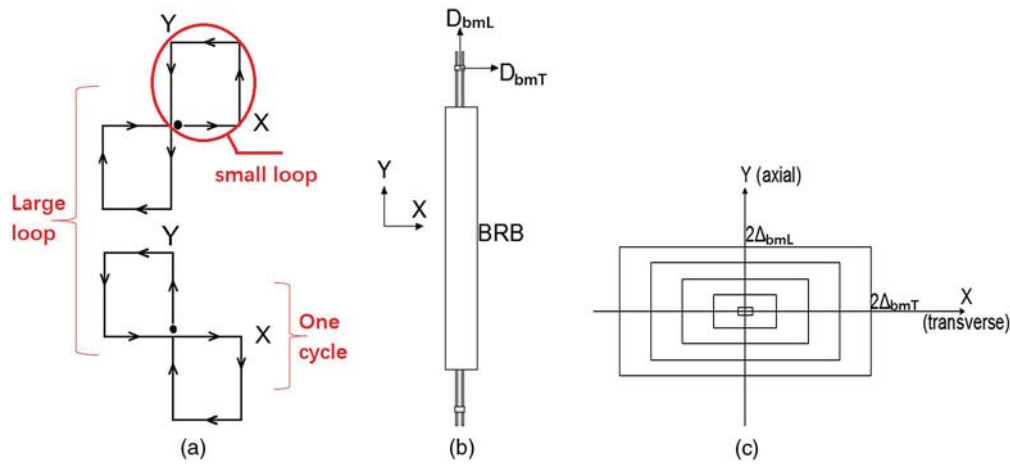


Fig. 6. Locations of (a) LPs; (b) LEDs in the test setup



**Fig. 7.** Biaxial s-type displacement pattern: (a) small loops with arrows of movement; (b) BRB's longitudinal and transverse demand; (c) movement of one end of the BRB (connected to the shake table)

respectively. The BRB is required to achieve a cumulative inelastic axial deformation of at least 200 times the yield displacement. For the application considered here, BRBs are explicitly expected to be subjected to significant out-of-plane deformations in addition to axial ones in the current proposed application in bidirectional EDS, the existing test protocol in AISC 341-10 had to be adapted. Bidirectionality was introduced in the test protocol by applying the biaxial S-type displacement pattern shown in Fig. 7(a). A complete large displacement loop is obtained by succession of the four small loops shown in Fig. 7(a), with movement of the shake table (looking from above) following the arrows.

The bidirectional BRB test was conducted by controlling the level of axial (longitudinal) and transverse displacement imposed on the BRB. Because AISC 341-10 specifies that the BRB's core plate must sustain progressively increasing axial displacements until a value equal to twice the axial design displacement  $D_{bmL}$ , it was therefore extrapolated here that it should also not fail at the twice the design displacement in both directions (transverse design displacement is denoted as  $D_{bmT}$ ). Each complete large loop in Fig. 7(c) was deemed equivalent to two of the cycles mentioned in the AISC test protocol because it imparted two full cycles of axial yield excursions. Therefore, at each displacement step of the AISC protocol outlined earlier, only one complete bidirectional large loop was needed. Similar to the AISC protocol, the displacement demands for each large loop were increased incrementally after completing the previous cycle, until  $2D_{bmL}$  and  $2D_{bmT}$  were reached in both directions. A constant strain rate of  $1.3 \times 10^{-3}/s$  was used for this test protocol (this test rate slightly changed for the adjusted bidirectional test protocols described later).

Because the end-connection performance for BRB-1 is dependent on the end plates' out-of-plane bending capacity, the objective for choosing the value of transverse design displacement  $D_{bmT}$  was to make sure that the end plates must not yield before  $D_{bmT}$  was applied to BRB-1s. The target transverse and longitudinal (i.e., axial) displacement demands of 40.69 mm (1.602 in.) and 16.41 mm (0.646 in.) were used as  $D_{bmT}$  and  $D_{bmL}$  in the bidirectional protocol. The bidirectional protocol's displacement versus time history is shown in Figs. 8(a and b), labeled as BD-E-I, for the longitudinal and transverse direction, respectively. When the BRB is subjected to the transverse displacement demand, as a result of the large amplitude of the displacements, this would also impose additional axial displacement demands to the BRB. Therefore, if the bidirectional protocol has maintained a constant longitudinal displacement

demand when the transverse displacements were applied, the BRB axial displacements would not have remained constant when it happened. To keep the axial BRB displacements constant (for sake of following the spirit of the AISC test protocol in the axial direction), the longitudinal displacement of the shake table was adjusted, as shown in Fig. 8(a).

Recall that, when obtaining the bidirectional displacement demands from the bridge model with generic BRBs, the ground motion producing the largest displacement demands at target ductility of 9 was selected as the reference motion. The decision of using the maximum displacement (resulting from all 22 pairs of ground motions) for the design target was revisited and found to be inconsistent with BRB design practice. This was because BRBs

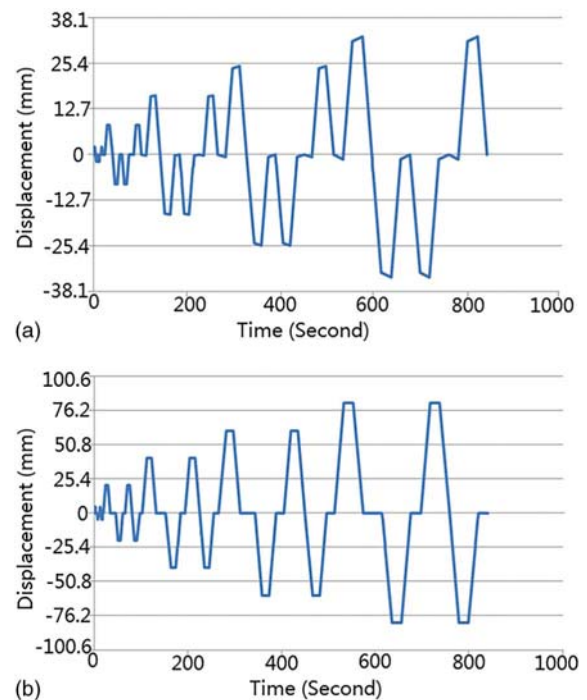


**Fig. 8.** Bidirectional qualification displacement history BD-E-I: (a) longitudinal displacement versus time; (b) transverse displacement versus time

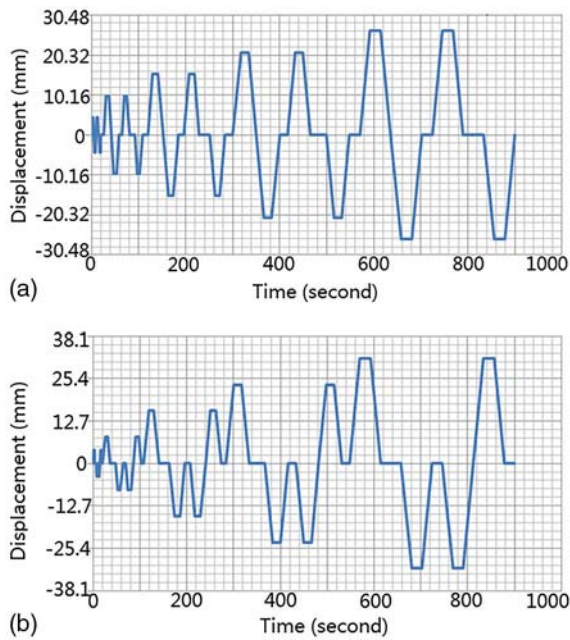


**Fig. 9.** Bidirectional qualification displacement history BD-A-I: (a) longitudinal displacement versus time; (b) transverse displacement versus time

are typically designed for twice the design displacements, which are representative of average response, and the multiplier of 2 is intended to account for maximum demands above the average. Therefore, for testing BRB-1, it was decided to use the average displacement, which was obtained from new nonlinear time-history analyses of the bridge model with the actual BRB-1 properties. To limit the cumulative inelastic displacements to approximately  $200D_{by}$  at the end of the bidirectional test, the target design ductility was reduced to 6, which gave the design longitudinal and transverse displacement demand of 1.11 cm (0.438 in.) and 1.57 cm (0.619 in.), respectively. The corresponding displacement versus time history of the new bidirectional test protocol is shown in Figs. 9(a and b), labeled BD-A-I, for the longitudinal and transverse direction, respectively.

### Axial Temperature-Induced Test Protocol

The low-cycle fatigue analysis results presented by Wei and Bruneau (2017) showed that the temperature history for Memphis, TN (for a given year) in Fig. 10(a) produced the most severe strain demand history on the BRB, and thus the smallest fatigue life for the 10 cities considered as part of that prior study. The strain history chosen also corresponds to the worst-case scenario for installation of the BRB at a temperature of 37.8°C (100°F), because doing so produces a temperature history that would put the BRB under mostly tensile strains, causing the BRB to approach fatigue faster, resulting in a shorter fatigue life. For a simply supported bridge model of 30.48 m (100 ft) with a longitudinal BRB installed with an inclination angle of 45° at one end, the resulting axial displacement demand history, named T-200-I, is shown in Fig. 10(b). The magnitude of the displacement history is 11.38 mm (0.448 in.), corresponding to a strain of 0.0096 and 0.0089 for BRB-1 and BRB-2, respectively. In principle, the number of times that the protocol in Fig. 10(b) would be applied to the BRB before failure gives the low-cycle fatigue life of that BRB in years, for the worst-case scenario considered.

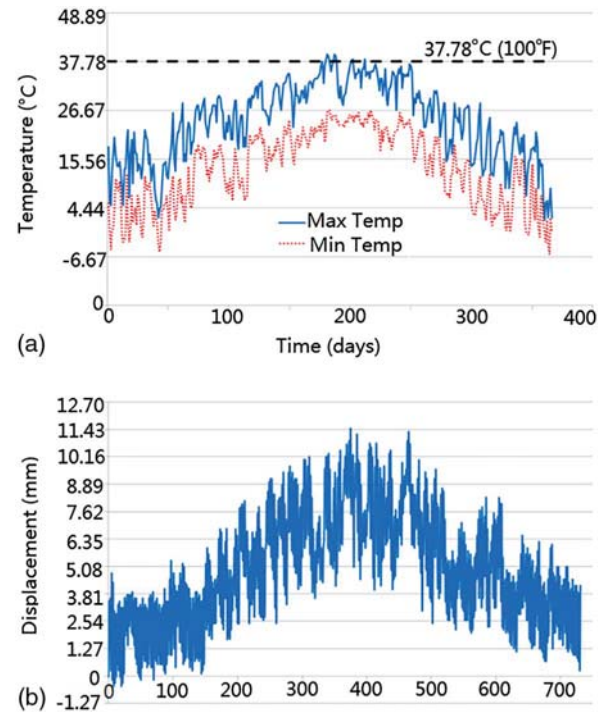


**Fig. 10.** (a) Recorded temperatures at Memphis, TN with BRB installation temperature of 37.78°C (100°F); (b) resulted axial displacement history T-200-I in the BRB core plate caused by 1 year of temperature changes (with respect with days in a year)

Recall that the bridge model with BRBs in EDS used to obtain the seismic demands, corresponds to a bridge of 30.48 m (100 ft) and has inclined longitudinal BRBs at both ends. Therefore, for consistency, if the temperature histories were to correspond to a similar span having expansion joints at both ends, the axial displacement demand history caused by temperature change shown in Fig. 10(b) would actually correspond to a bridge of 60.96 m (200 ft). The BRB-2s specimens, which were subjected to this axial displacement history, were actually tested for twice the axial displacement demand because of the temperature-change effect that would be experienced on a 30.48-m (100-ft) span bridge. The adjusted correct axial displacement history, corresponding to a 30.48-m (100-ft) bridge, was applied to the BRB-1 specimens.

### Combined Protocols Used in BRB Tests

The test protocols described earlier served as templates for the bidirectional qualification test and temperature-induced axial test. Various combinations of these protocols were considered and combined to provide a broader understanding of the expected behavior and service life for both types of BRBs. Four specimens of each type of BRB were tested. The different combinations of displacement protocols that were applied are summarized in Table 1. The four BRB-2 specimens were first tested. In all tests, the number of cycles to which the BRBs were subjected prior to failure was recorded, with the goal of estimating their service life. The number of years in parentheses in Table 1 for the axial displacement history implies the repeated numbers of times that the yearly displacement history was applied to the specimen. During testing, a complication arose because of the presence of gaps at the BRB's end connections and also to the flexibility of the test setup (elastic deformations and slippage of the reaction blocks caused by initial anchorage problems); both bidirectional and axial displacement histories were adjusted accordingly. The specifics for those protocol changes

**Table 1.** Summary of BRB Test Protocols

Specimen	Test protocol				
	Test A	Test B	Test C	Test D	Test E
BRB-2-1 <sup>a</sup>	BD-E-I (to $1.5D_{bmL}$ )	BD-E-I	BD-E-II	—	—
BRB-2-2 <sup>b</sup>	T-200-I (85 years)	$T-200-I \times 1.5$ (10 years)	$T-100-I \times 1.75$ (9 years)	—	—
BRB-2-3 <sup>c</sup>	BD-E-III	T-200-II (5 years)	Axial trial	T-200-II (10 years)	BD-E-III (partial)
BRB-2-4	T-200-II (15 years)	BD-E-III	—	—	—
BRB-1-1 <sup>d</sup>	BD-A-I	T-100-I (75 years)	$T-200-I \times 1.37$ (10 years)	$T-200-I \times 2.05$ (10 years)	—
BRB-1-2 <sup>e</sup>	BD-A-I	T-100-II	T-5 (33 years)	—	—
BRB-1-3 <sup>f</sup>	BD-A-II	BD-A-2%	BD-A-4%	BD-A-6%	—
BRB-1-4 <sup>g</sup>	BD-N	T-5 (35 years)	BD-N	BD-N-G (five times)	—

<sup>a</sup>Bidirectional qualification testing with BD-E-I was stopped after finishing the cycle corresponding 1.5 times the design displacement to secure the fixture of the reaction block on the strong floor to prevent large slippage; BD-E-II was modified from BD-E-I with only the cycle corresponding to the transverse displacement demand  $2.5D_{bmT}$  and longitudinal displacement demand  $2D_{bmL}$ .

<sup>b</sup> $T-200-I \times j$  ( $k$  years) indicates that T-200-I was magnified by  $j$  times to apply to the BRB for  $k$  years in order to fail the BRB faster after finish the required years of temperature history.

<sup>c</sup>BD-E-III was increased from BD-E-I in the longitudinal direction to include the flexibility of the test setup plus the pin slippage at the BRB's end to ensure the intended displacement demands could be applied to the BRB's core plate; T-200-II was also increased from T-200-I to consider this adjustment. A-I was a trial axial test to ensure the slippage of the reaction block on the shake table was reduced to acceptable values.

<sup>d</sup>T-100-I is the temperature-induced axial displacement history corresponding to a 30.48 m (100 ft) bridge with increased amplitude to account for the flexibility of the test setup plus the bolt slippage at the BRB's end.

<sup>e</sup>T-100-II is the magnified T-100-I with the increased sampling rate and reduced test speed to capture the BRB's hysteretic curve, and T-5 is the resulting history which put the BRB under the inelastic deformation of five times yield displacement in 1 year.

<sup>f</sup>BD-A-II is the average bidirectional qualification test history without longitudinal displacement adjustment; BD-A- $m\%$  means the bidirectional protocol with transverse and longitudinal demand of  $m$  inches and  $1.5D_{bmL}$  in BD-A-II, respectively.

<sup>g</sup>BD-N-G and BD-N stand for the actual bidirectional displacement trace of the BRB's response to an actual ground excitation obtained from the bridge model with and without the bolt gap at the ends.

[details presented in Wei and Bruneau (2016)] are not described here because of length considerations.

### BRBs' Hysteretic Behaviors

The tests conducted for each BRB specimens are described next, focusing on the hysteretic curves of the BRB under each type of loading. The naming of the different tests, BRB- $i$ - $j$ - $X$ , refers to test  $X$  in Table 1 performed on specimen BRB- $i$ - $j$ , which is the  $j$ th specimen of BRB type  $i$ .

BRB-2-1 was subjected to bidirectional displacement protocol BD-E-I, and the corresponding hysteretic curve of BRB-2-1's axial force versus axial deformations measured by LPs is shown in Fig. 11(a). After slippage of the reaction block on the strong floor was fixed, BRB-2-1-B was subjected to BD-E-I again, and the corresponding hysteretic curve of its axial force versus deformations measured by LPs is shown in Fig. 11(b). After completion of the first incomplete bidirectional qualification test and subsequent complete one using Protocol BRB-E-I, BRB-2-1 had not failed. It was subjected to a new protocol of additional displacement histories BD-E-II to investigate the BRB's ultimate transverse displacement capacity. BD-E-II, with increased transverse displacement demand at  $2.5D_{bmT}$ , was applied to BRB-2-1 in Test BRB-2-1-C. BRB-2-1 failed before finishing BRB-E-II, and the corresponding hysteretic curve is shown in Fig. 11(b) by the dotted line (i.e., at  $2.5D_{bmT}$ ), superposed on top of the largest displacement cycle (i.e., at  $2D_{bmT}$ ) applied during Test BRB-2-1-B [in Fig. 11(a)] for comparison.

BRB-2-2 was subjected only to temperature-induced axial displacement histories. Because of the fast speed of the input axial displacement history, the force output of the shake table was affected by the inertia of the shake table and could not reflect the force in the BRB in real time when using a data output frequency

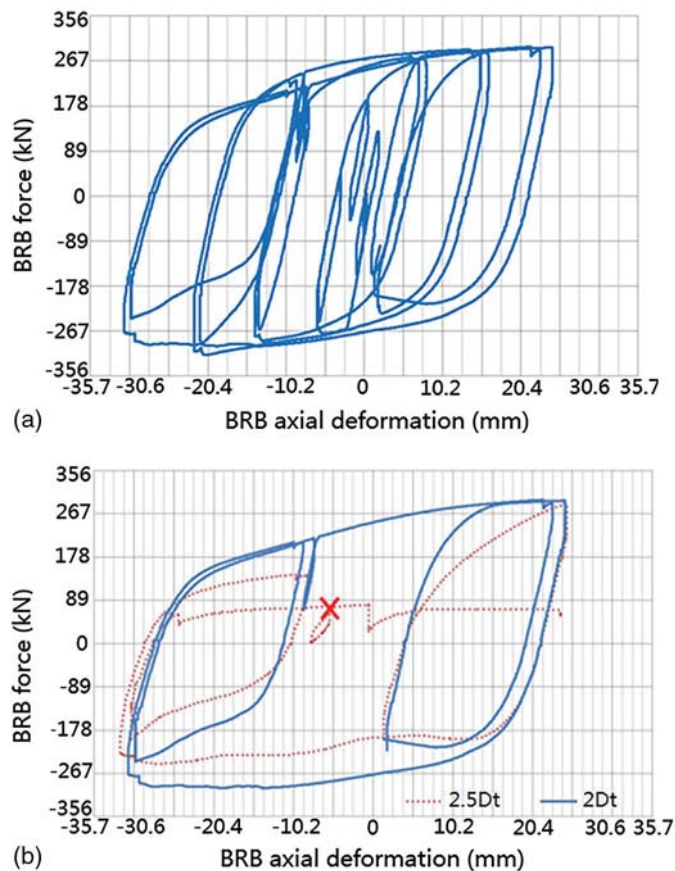


**Fig. 11.** BRB-2-1's axial force versus deformation subjected to (a) BD-E-I in Test BRB-2-1-B; (b) BD-E-II in Test BRB-2-1-C (compared with largest cycle in BD-E-I)

of 32 Hz. The maximum sampling rate of the Krypton system is 32 Hz, and the frequency of the data acquisition from the LPs and SPs was also kept at 32 Hz for consistency, which was not large enough to accurately capture the change in displacements. Therefore, the recorded hysteretic curves of the BRB's force versus axial deformation could not reflect the BRB's real hysteretic behavior. This problem only occurred in the temperature-induced displacement histories because the sampling rate was adequate for the bidirectional qualification test (which led to reliable plot of the BRB's axial forces versus axial deformation in that case). BRB-1s were tested by doubling the sampling rate of the shake table and potentiometers, as well as reducing the input speed of the displacement history. Because of length concerns, only the results for BRB-2-2 under this axial temperature-induced history are presented here for the BRB-2 type. Details of results for the other BRB-2s tests can be found in Wei and Bruneau (2016).

Axial displacement Protocol T-200-I was first applied to the specimen in Test BRB-2-2-A for 85 times (i.e., corresponding to 85 years of temperature changes). Fig. 12(a) shows the corresponding hysteretic curve of the BRB's axial force versus the table's longitudinal displacement output for the first five cycles of temperature-induced axial displacement histories (i.e., for 5 years of temperature changes). The table's longitudinal direction was the same as the BRB's axial direction. Except for the first cycle when the BRB was loaded from zero deformation and axial force, the other four cycles followed the same shape as shown in Figs. 12(b and c), which compares the table's longitudinal displacement output and the BRB's applied axial displacement under the same five cycles of T-200-I. The differences in displacement range between them were caused by sliding displacement of the reaction blocks on the shake table and strong floor, as well as the deformation of the reaction blocks under the BRB's force. Fig. 12(d) compares the BRB's axial deformation and the BRB's applied axial displacement for the same five cycles, and the difference in Fig. 12(d) was attributable to the pin gap in the BRB's end connections with the gusset plates in the reaction blocks. Because BRB-2-2 was unfailed after 85 cycles, T-200-I was arbitrarily scaled up by 1.5 times and successfully applied to the specimen for 10 cycles in Test BRB-2-2-B. Then, T-200-I was scaled up to 1.75 times the original amplitude, with the intention of applying it to the specimen until failure. BRB-2-2 sustained nine cycles of this final temperature displacement history, and failed at beginning of the 10th cycle. The BRB force versus shake table's longitudinal displacement for these nine cycles in Test BRB-2-1-C is shown in Fig. 12(e). In the 10th cycle, BRB-2-2 failed at the displacement marked as shown in Figs. 12(f and g), which compares the BRB's axial deformation and the BRB's applied axial displacement for these 10 cycles.

Based on tests of previous BRB-2s, BD-E-I and T-200-I were modified as BD-E-III and T-200-II, respectively, to take into account the elastic deformations of the reaction blocks, as well as pin slippage (to reflect demands in BRBs that would have slip-resistant bolted connections instead of single pin/bolt connections). BRB-2-3 and BRB-2-4 were both subjected to bidirectional qualification test history and temperature-induced axial displacement histories in different sequence with the intent to investigate how the seismic demands affected the service life of the BRB. In Test BRB-2-3-A under BD-E-II, the corresponding hysteretic curve of the BRB's axial force versus deformation is shown in Fig. 13(a). T-200-II was applied to the BRB-2-3 for five cycles in Test BRB-2-3-B. After the reaction block's anchorage to the shake table was fixed, Test BRB-2-3-C was performed to make sure that sliding of the reaction block on the shake table was reduced to an insignificant

level, and the corresponding hysteretic curve of BRB-2-3's axial force versus axial deformation is shown in Fig. 13(b).

BRB-2-3 was then subjected to five supplementary cycles of the T-200-II in Test BRB-2-3-D. Because BRB-2-3 was not subjected to the full magnitude of the intended displacement demand in Test BRB-2-3-A because of the slippage of the reaction block on the shake table, it was retested only for the cycle at a displacement magnitude corresponding to twice the design displacement in BD-E-III. In this Test BRB-2-3-E, the BRB failed during at the second small loop in tension when the table was moving longitudinally to the largest displacement of  $2D_{bmL}$ . The corresponding hysteretic curve of BRB-2-3's axial force versus axial deformation is shown in Fig. 13(c). For tests of BRB-2-4, a total of 15 cycles of the axial displacement protocol T-200-II was first applied to BRB-2-4 in Test BRB-2-4-A. The specimen was subjected to the bidirectional displacement Protocol BD-E-III in Test BRB-2-4-B, but failed during the largest cycle, corresponding to twice the design displacement. The corresponding hysteretic curve of BRB-2-4's force versus axial deformation is shown in Fig. 13(d).

BRB-1-1 was subjected to the BD-A-I in Test BRB-1-1-A, and the resulting hysteretic curve of the BRB's axial force versus axial displacement is shown in Fig. 14(a). In Test BRB-1-1-B, the temperature-induced axial displacement history T-100-I in Fig. 14(b), which corresponds to a 30.48 m (100 ft) long bridge and includes the elastic deformation of the reaction blocks and the bolt slippage, was applied to BRB-1-1 for 75 cycles, and the corresponding hysteretic curve of BRB-1-1's axial force versus table's longitudinal displacement output for 10 cycles is shown in Fig. 14(c). Fig. 14(d) compares the BRB's axial deformation and applied axial displacement for the same 10 cycles. The bolt gap in BRB-1's connection is 6.86 mm (0.27 in.), which is larger than the value of 1.59 mm (0.0625 in.) for BRB-2s. To complete testing of the specimen already in place, T-100-I was arbitrarily scaled up to 1.37 times and applied to the specimen for 10 cycles in Test BRB-1-1-C. After that, BRB-1-1 was subjected to a further amplified axial displacement history, scaled up to 2.05 times from the T-100-I and used in Test BRB-2-2-D. The specimen completed three cycles of this displacement history and failed during the fourth cycle. The corresponding BRB axial force versus table longitudinal displacement for these four cycles is shown in Figs. 14(e and f), which compares the BRB's axial deformation and applied axial displacement for these four cycles.

BRB-1-2 was first subjected to BD-A-I in Test BRB-1-2-A, and the corresponding hysteretic curve of BRB-1-2's axial force versus axial deformation is shown in Fig. 15(a). The sampling rate in the data acquisition system was increased, and BRB-1-2 was subjected to two cycles of T-100-I. Hysteretic curves of axial force versus axial deformation from previous BRB tests show that the total displacement magnitude of the axial displacement history mattered more than the small cycles (for which strains in the BRB remained in the elastic range). Therefore, the magnitude of the axial displacement history was arbitrarily increased, such as to produce an inelastic BRB deformation of approximately 2.5 times the yield displacement of the BRB. The revised temperature-related axial displacement history in Fig. 15(b), namely T-5, was set with a range of 19.56 mm (0.77 in.). To achieve the intended BRB inelastic deformations and satisfactory data resolution, the test duration for that protocol was doubled, and the resulting displacement history was applied to the specimen for one cycle for verification in Test BRB-1-2-B.

Fig. 15(c) shows the corresponding hysteretic curve of BRB's axial force versus axial displacement, and the dashed line indicates an approximate bilinear envelope for the resulting hysteretic curve. This envelope is shaped to match the slopes of the elastic

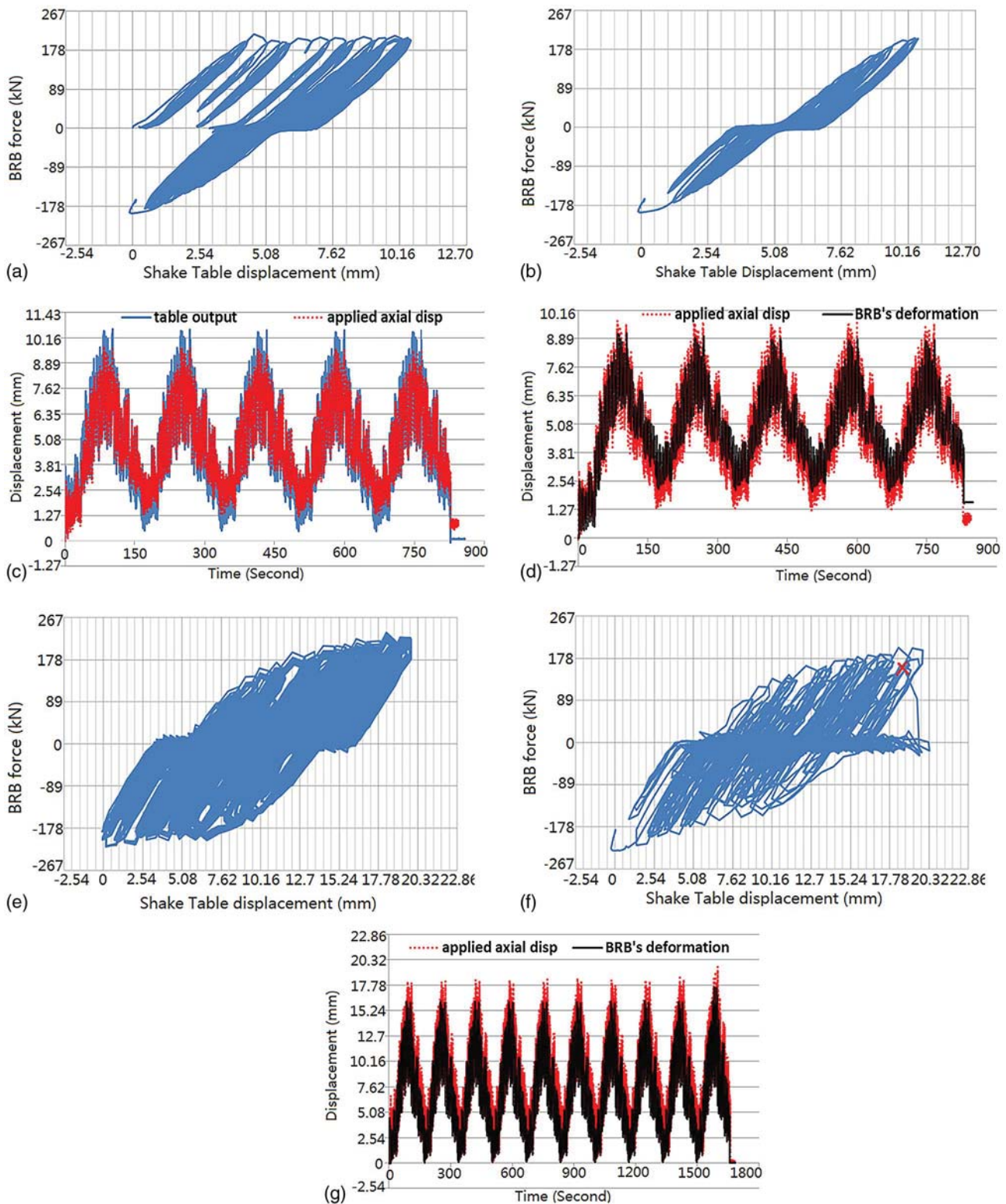


**Fig. 12.** BRB-2-2 behaviors: BRB axial force versus longitudinal table displacement for (a) the first five cycles in test BRB-2-2-A and (b) typical one cycle in Test BRB-2-2-A; (c) shake table's longitudinal displacement output and applied axial displacement comparison for the first five cycles in Test BRB-2-2-A; (d) axial deformation and applied axial displacement comparison for the first five cycles in Test BRB-2-2-A; BRB axial force versus longitudinal table displacement comparison for (e) 10 cycles in Test BRB-2-2-C, (f) last cycle in Test BRB-2-2-C, and (g) axial deformation and applied axial displacement comparison for the 10 cycles in Test BRB-2-2-C

deformation and peaks in the total deformation. The left and right dashed lines match the elastic part with twice the yield displacement, and the upper and lower dashed lines approximately connect the peaks of the elastic deformation. The total inelastic deformation

to which the BRB was subjected under this one cycle of temperature-related displacement history, is 5.34 times the BRB's yield displacement. The displacement history T-5 was applied to BRB-1-2 until failure and the specimen failed at the 33rd cycle

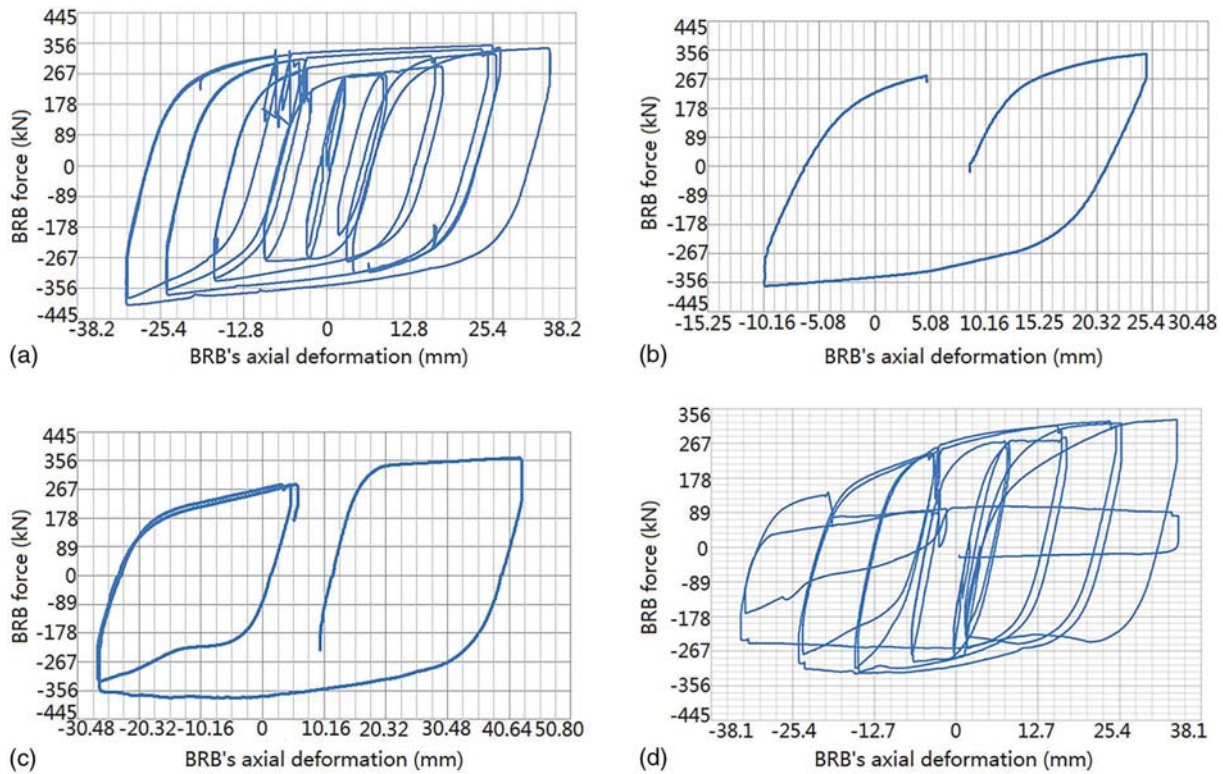


**Fig. 13.** BRB-2-3 and BRB-2-4 behaviors: (a) BRB-2-3's axial force versus deformation subjected to BD-E-II in Test BRB-2-3-A; (b) BRB axial force versus longitudinal table displacement for typical one cycle in Test BRB-2-3-B; (c) BRB-2-3's axial force versus deformation subjected to largest cycle in BD-E-II in Test BRB-2-3-E; (d) BRB-2-4's axial force versus deformation subjected to BD-E-III in Test BRB-2-4-B

when the displacement was at the maximum. The corresponding hysteretic curve of BRB-1-2's axial force versus axial deformation for the last cycle is shown in Fig. 15(d).

BRB-1-3 was only subjected to bidirectional displacement histories. Bidirectional displacement history BD-A-II [longitudinal displacement history shown in Fig. 16(a)], modified by removing the longitudinal displacement adjustments from BD-A-I, was applied to BRB-1-3 in Test BRB-1-3-A, and the corresponding hysteretic curve of BRB-2-4's force versus axial deformation is shown in Fig. 16(b). In order to explore the transverse displacement capacity of the BRB, the BD-A-II was revised to impose arbitrary transverse displacement demands progressively increasing to 50.8 mm (2 in.), 101.6 mm (4 in.), and 152.4 mm (6 in.), while the longitudinal displacement demand remained at 1.5 times the design displacement. The displacement histories shown in Fig. 16(c) corresponding to transverse displacement demands of 50.8 mm (2 in.), 101.6 mm (4 in.), and 152.4 mm (6 in.), were named BD-A-2%, BD-A-4%, and BD-A-6%, respectively. In Test BRB-1-3-B, BD-A-2%, BD-A-4%, and BD-A-6% were applied to the specimen sequentially for one cycle each. The corresponding hysteretic behaviors of BRB-1-3 subjected to BD-A-2%, BD-A-4%, and BD-A-6% are shown in Figs. 16(d-f), with axial deformation measured by LPs and the Krypton system given by dotted and solid lines, respectively. The BRB experienced unloading and reloading in the circled part, which is attributable to added axial deformation at the large transverse displacement demand.

The bidirectional displacement histories used for the previous BRB tests all followed a rectangular trace, sequentially applying longitudinal and transverse displacement, effectively enveloping the actual seismic displacement response of the BRB in the simplified bridge diaphragm model. In the bidirectional test of

BRB-1-4, the movement of the shake table followed the actual bidirectional displacement trace of the BRB's response when subjected to a ground excitation, instead of the rectangular envelope. The bidirectional displacement history BD-N in Fig. 17(a) corresponds to the design displacement demand in BD-A-I and takes into account the elastic deformations of the reaction blocks plus the bolt slippage. The corresponding hysteretic curve of BRB-1-4's axial force versus axial deformation in Test BRB-1-4 subjected to BD-N is shown in Fig. 17(b). BRB-1-4 was subjected to BD-N again in Test BRB-1-4-C, and the corresponding hysteretic curve of the BRB's axial force versus axial deformation is shown in Fig. 17(c).

To investigate how the existence of the bolt gaps affected the dynamic response of the BRB, the bolt gaps were included in the simplified bridge diaphragm model, with the intent of obtaining a displacement history representative of the BRB's response that could develop when gaps were present at the bolts. For this purpose, an elastic perfectly plastic gap (EPPG) material was used to model the bolt gaps (together with the BRB), which replaced the bilinear material of the BRB. The resulting bidirectional displacement history, namely BD-N-G-C, is shown in Fig. 18(e). Because of uncertainty in the direction of any input ground motion, the displacement demand history could equally have been the one shown in Fig. 17(e), namely BD-N-G-T (if the ground motion directions had been inverted), which would subject the BRB to more tension than compression. In Test BRB-1-4-D, bidirectional displacement histories BD-N-G-C and BD-N-G-T were successively applied to the specimen, alternating one after the other until failure. BRB-1-4 failed during the third repetition of the BD-N-G-T (in other words, after three cycles of BD-N-G-C and two cycles of BD-N-G-T). The comparisons of hysteretic curves of BRB-1-4

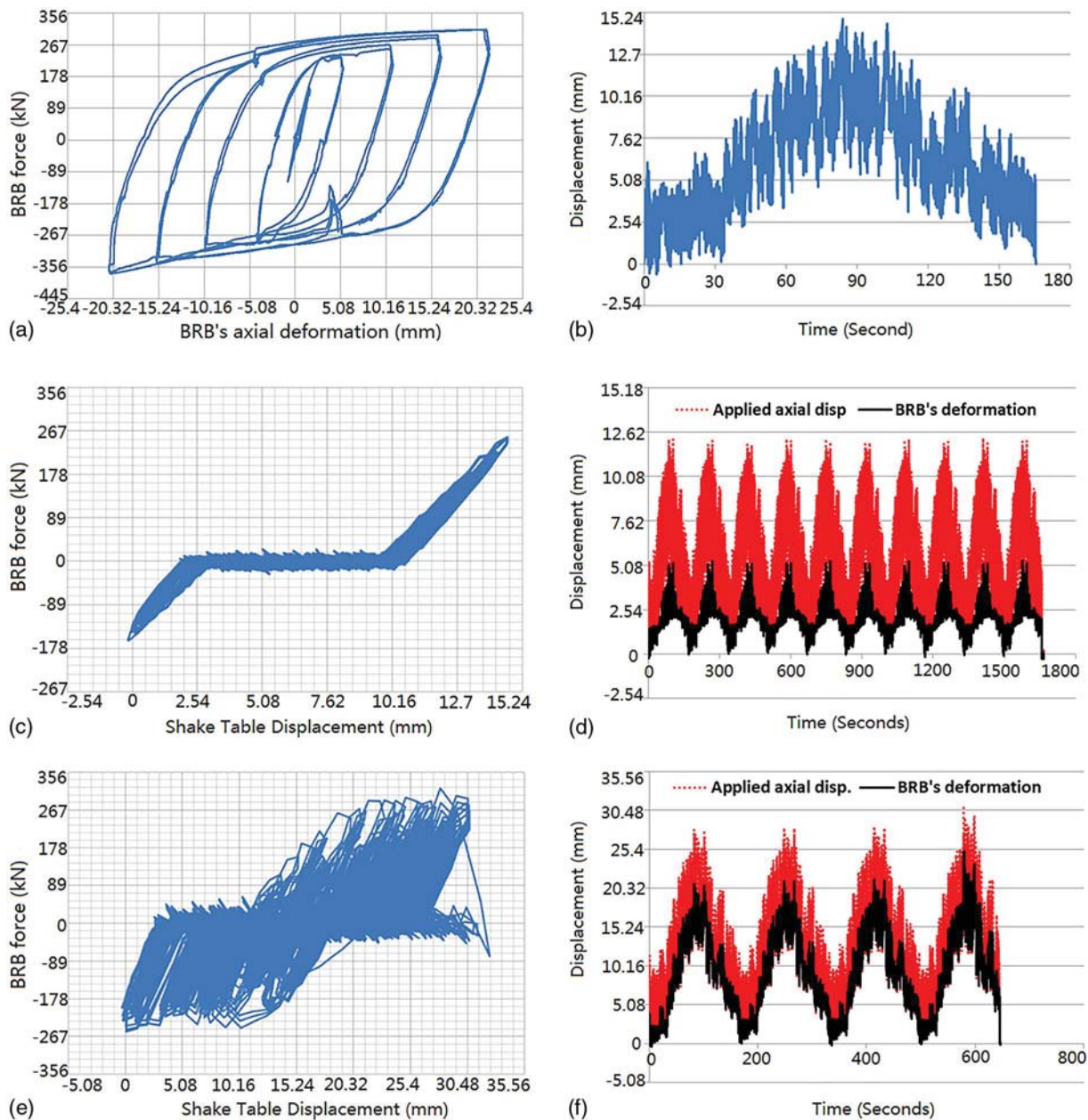


**Fig. 14.** BRB-1-1: (a) BRB-1-1's axial force versus deformation subjected to BD-A-I in Test BRB-1-1-A; (b) temperature-induced axial displacement history T-100-I; (c) BRB axial force versus longitudinal table displacement for 10 cycles in Test BRB-1-1-B; (d) axial deformation and applied axial displacement comparison for 10 cycles in Test BRB-1-1-B; (e) BRB axial force versus longitudinal table displacement for four cycles in Test BRB-1-1-D; (f) axial deformation and applied axial displacement comparison for four cycles in Test BRB-1-1-D

under these two bidirectional displacement histories obtained considering the bolt gap slippage are shown in Fig. 17(f), with a dotted line and solid line for BD-N-G-C and BD-N-G-T, respectively.

## Evaluation of BRBs' Performance

### Observations on BRBs' Failure

As expected, all the BRBs failed in tension after extensive cycles of inelastic deformation, irrespective of whether the BRB was subjected to bidirectional or temperature-induced axial displacement histories. No end-plate failure or instability was observed.

After the test, a visible bulge at one end of the BRB was observed in almost all BRBs, except for BRB-2-2, which was only subjected to uniaxial displacement histories caused by temperature change. Fig. 18(a) shows a typical bulge at the northeast side of BRB-2-4 when viewed from the direction (solid line) shown by the arrow in Fig. 18(b). For different BRBs, the bulges occurred on different sides (east and west) and ends (north and south), as documented in Table 2 (in that table, NE, SE, and SW stand for the northeast, southeast, and southwest sides of the BRB, and N/A means no apparent bulge was observed). After opening some BRB specimens (cutting the casing with a cutting torch, and chipping the concrete with a small hammer and a chisel), it was found that the bulge was produced by the core plate's buckling inside the concrete and HSS at that location.

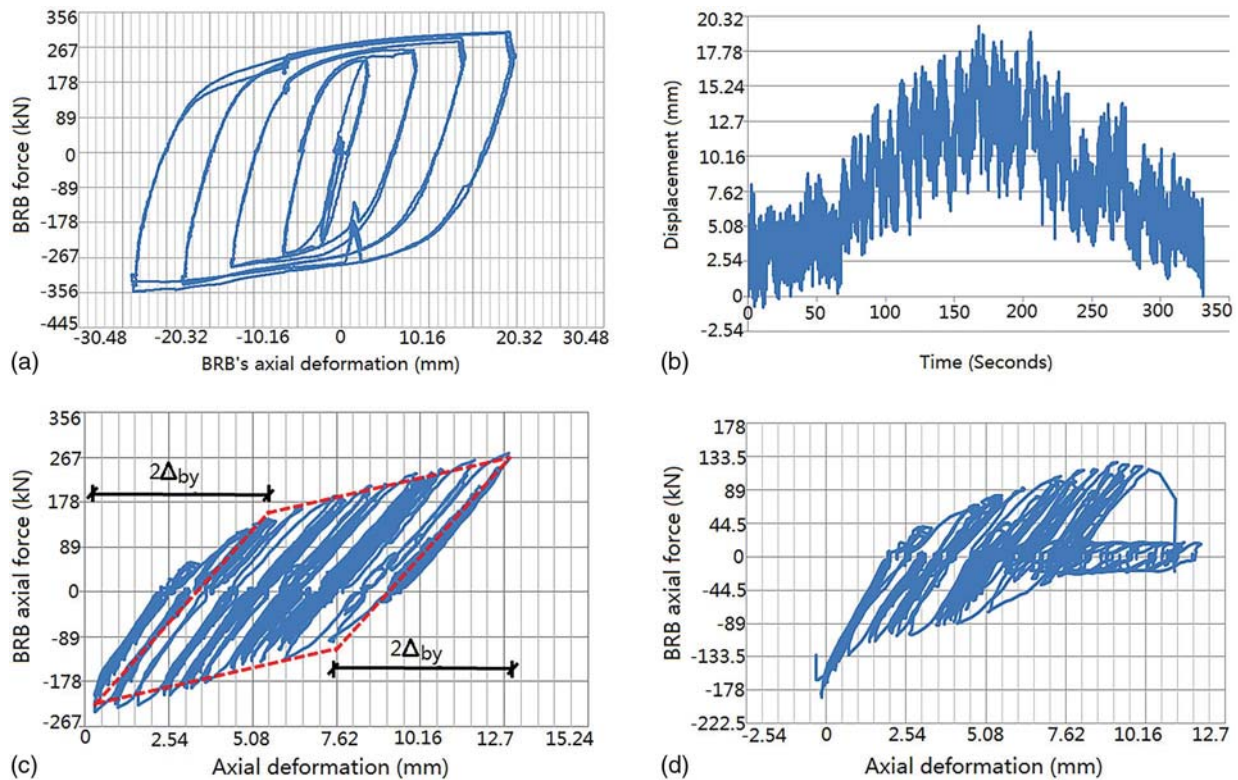


**Fig. 15.** BRB-1-2: (a) BRB-1-2's axial force versus deformation subjected to BD-A-I in Test BRB-1-2-A; (b) temperature-induced axial displacement history T-5; BRB axial force versus BRB's axial deformation for (c) typical cycle in Tests BRB-1-2-B and BRB-1-2-C, and (d) last cycle in Test BRB-1-2-C

For some BRBs, the HSS casing was cut open where the bulge was the largest, revealing the displaced (and cracked) concrete inside, as shown in Fig. 19(a) (for BRB-2-4 as an example). That cracked concrete was then partly removed to reveal the steel core. Fig. 19(b) shows the fractured core plate when viewed from the direction (dashed line) shown by the arrow in Fig. 18(b). Visibly, significant out-of-plane displacement of the core plate had occurred and was the cause of the observed bulges. After completely removing the collar, HSS casing, and encased concrete, the entire core plate was revealed. Fig. 19(c) shows part of the core plate in the vicinity of where it fractured. That fracture occurred at the tip of a severe and isolated local buckle. The circled part of the core plate shown in Fig. 19(c) is similarly circled in Fig. 19(d) to show that failure typically occurred in the part of the core plate close to the transition zone [typically at one of the two locations as shown in Fig. 19(d)]. When fracture occurred at one of the two circled location in Fig. 19(d), at the opposite location close to the other transition part of the core plate, significant out-of-plane deformation of the core plate also happened, but it had smaller amplitude than where failure occurred. Specific manufacturing details of the tested BRB (which are proprietary and cannot be revealed) were found to explain why the BRB core plate could more easily buckle at those two locations, and recommendations were made to the BRB manufacturers that could enhance the low fatigue life of the BRB (although one must keep in mind that all the BRBs already exhibited considerable cumulative ductilities, as shown in the section "Cumulative Inelastic Displacements"). Except for these two circled part in Fig. 19(d), the rest of the core plate remained mostly straight (verified using a straight edge).

### Cumulative Inelastic Displacements

A commonly used approach to quantify the severity of each BRB's inelastic response under different displacement history in each test

is to examine the cumulative inelastic deformations that the BRB experienced. In Table 3, the cumulative inelastic deformations are quantified in terms of the axial yield displacement of the BRB,  $\Delta_{by}$ . Recall that the yield displacements  $\Delta_{by}$  are 2.72 mm (0.107 in.) and 2.06 mm (0.081 in.) for BRB-1 and BRB-2, respectively. All the BRBs developed cumulative inelastic displacement of more than  $200\Delta_{by}$ , which is a threshold of inelastic performance specified as part of the acceptance criteria in AISC 341-10 specifications. The different test protocols used for the various specimens tested (and sequence in which these protocols were applied) partly explain the differences in cumulative inelastic displacements recorded for each of the BRBs in Table 3.

The following observations can be made based on the comparisons of cumulative inelastic deformations among different BRBs:

- When comparing results for BRB-1-3 and BRB-2-1, which were both only subjected to bidirectional displacement histories (i.e., without temperature-induced demand), it was observed that BRB-1-3's cumulative inelastic deformation is larger than that of BRB-2-1. Given that the bidirectional test displacement histories for BRB-1 generally had smaller amplitude than for BRB-2, this indicates that the BRBs failed after fewer cycles of inelastic deformations when those cycles were of a larger amplitude, which resulted in smaller cumulative inelastic deformations;
- When comparing results for BRB-1-1 and BRB-1-2, which were both first subjected to essentially the same bidirectional displacement history followed by different axial temperature-induced displacement histories until failure, it was observed that the BRB subject to a larger amplitude of axial displacement history failed at a smaller cumulative inelastic deformation. Large amplitudes of axial displacement history were used at the end in Test BRB-1-1-D to fail the BRB specimen. The maximum amplitude of the axial displacement history used for

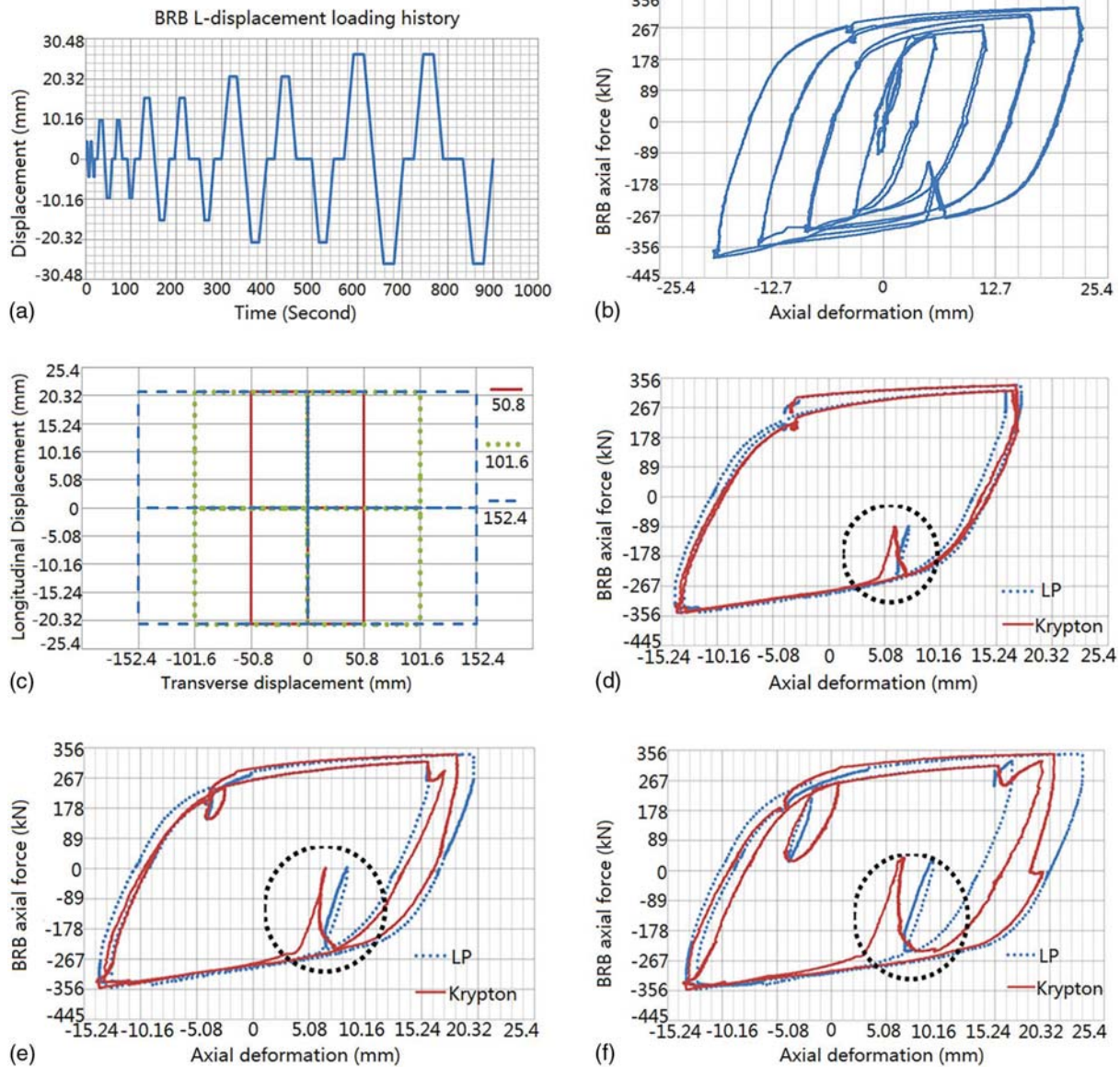


**Fig. 16.** BRB-1-3: (a) longitudinal displacement history in BD-A-II; (b) BRB-1-3's axial force versus deformation subjected to BD-A-II in Test BRB-1-3-A; (c) bidirectional displacement history BD-A-2%, BD-A-4%, and BD-A-6%; BRB-1-3's axial force versus deformation subjected to (d) BD-A-2% in Test BRB-1-3-B; (e) BD-A-4% in Test BRB-1-3-B; (f) BD-A-6% in Test BRB-1-3-B

BRB-1-2 was 64% of that for BRB-1-1, and it sustained 86% more of inelastic deformation under the axial temperature-induced displacement; and

- BRBs were observed to fail at smaller cumulative inelastic deformation values if they experienced many years of the small temperature-induced axial displacement demand before the bidirectional displacement demands from the earthquake was applied. This can be seen by comparing results for BRB-2-3 and BRB-2-4. Multiple cycles of T-200-III (corresponding to  $60\Delta_{by}$ ) were first applied to BRB-2-4 before BD-E-III (corresponding to  $200\Delta_{by}$ ) was applied. In the test of BRB-2-3, the BRB was first subjected to BD-E-III (corresponding to  $245\Delta_{by}$ ), followed then by a different number of cycles of T-200-II (corresponding to  $44\Delta_{by}$ ), and ended with more cycles of partial BD-E-III (corresponding to  $118\Delta_{by}$ ). BRB-2-3 reached 156% more cumulative inelastic deformation than BRB-2-4. This result suggests that the sequence in which the different displacement histories are applied could matter.

All the BRBs reached cumulative inelastic deformations of  $250\Delta_{by}$ , except for BRB-1-1. In BRB-1-1, which reached only  $222\Delta_{by}$ , the temperature-induced axial displacement history was scaled up to a large magnitude at the end of the test, with the intention to fail BRB-1-1 quicker, and it is possible that this reduced the fatigue life. However, more tests would be needed to provide a statistical basis to validate these observations. Although the BRBs were identical in their design, some subtle (but not easily visible) differences in how they were fabricated could also be responsible for the observed differences.

From a design perspective, the presented information could be used to assess how many years a BRB could remain in service while retaining its ability to provide adequate seismic response. For example, for a bridge with the length,  $L$ , in Memphis, TN installed with longitudinal BRBs having a steel core length of 6% with no inclination (i.e., installed horizontally) at each end in the EDS, the number of years depends on BRB's design displacement demand from the earthquake (which is chosen to correspond

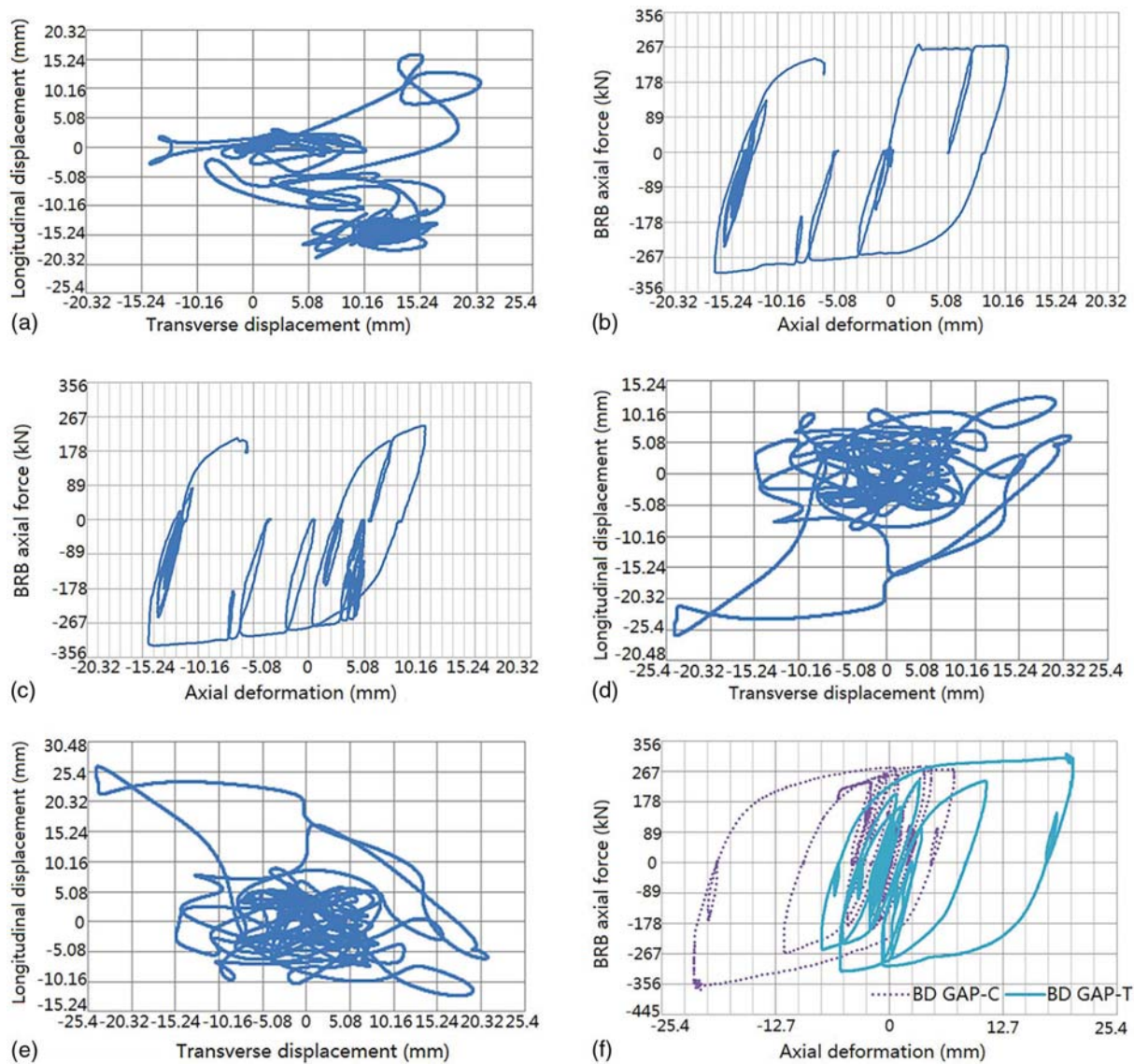


**Fig. 17.** BRB-1-4: (a) longitudinal versus transverse displacement trace in BD-N; BRB-1-4's axial force versus deformation subjected to (b) BD-N in Test BRB-1-4-A and (c) BD-N in Test BRB-1-4-C; longitudinal versus transverse displacement trace in (d) BD-N-G-C and (e) BD-N-G-T; (f) BRB-1-4's axial force versus deformation subjected to BD-N-G-C and BD-N-G-T in Test BRB-1-4-D

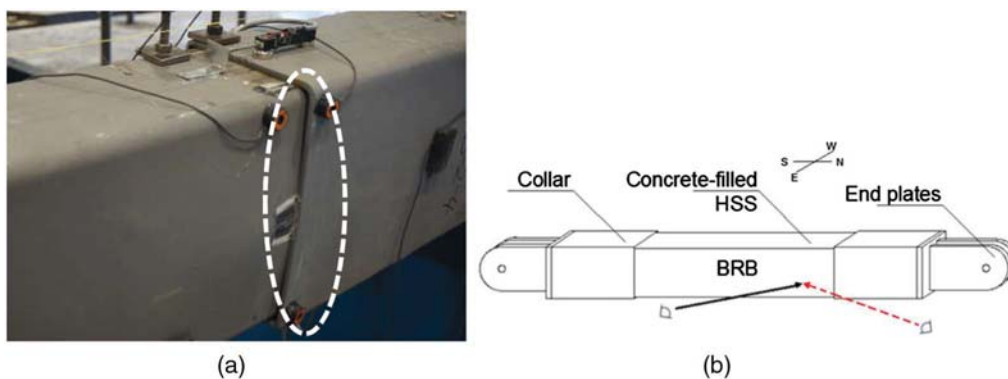


**Fig. 18.** Bulge on the NE side of the HSS of BRB-2-4

to a ductility,  $\mu_B$ , of 6 in this example). The cumulative inelastic deformation in the AISC axial qualification test protocol equals to  $8 \times (5\mu_B - 4)$ , which gives  $208\Delta_{by}$  for a ductility of 6. If the maximum cumulative inelastic deformation of the BRB of  $250\Delta_{by}$  is

used here, this leaves  $42\Delta_{by}$  available for the cumulative inelastic deformations of the BRB subjected to the temperature displacement history. For a BRB steel core plate having yield strength and Young's modulus of 317.2 MPa (46 ksi) and 200 GPa

**Table 2.** Summary of BRB Bulges after Failure

BRB	Side
2-1	NE
2-2	N/A
2-3	NE
2-4	NE
1-1	SE
1-2	NE
1-3	SE
1-4	SW

(29,000 ksi), the yield displacement of the BRB based on deformation only in the core length,  $\Delta_{by}$ , equal to  $9.52 \times 10^{-5} L$  (i.e., equal to  $46/29,000 \times 0.06L$ ).

For the case at hand (Memphis), the maximum and minimum yearly temperatures are 38.9°C (102°F) and -6.7°C (20°F), and the temperature range,  $\Delta T$ , is 27.8°C (82°F) [for 2012, from Fig. 17(a)]. Assuming that the bridge's concrete slab governs its thermal expansion, and using the coefficient of thermal expansion of concrete,  $\alpha_c$ , of 0.000006 m/m/°F (in./in./°F) to calculate the 1-year temperature displacement history applied to the BRB as  $0.5\alpha_c L \Delta T$  (tributary length of the bridge for each longitudinal BRB is  $0.5L$ ). The corresponding inelastic deformation of the BRB is  $\alpha_c L \Delta T - 4\Delta_{by}$ , equaling to  $1.17\Delta_{by}$ . Therefore, the number of years that the BRB can be installed in the EDS of this bridge is approximately 35 years. The number of years in service would be greater if gaps in the end connections of the BRB absorbed some of these thermal displacements.

### Low-Cycle Fatigue Damage

In this section, the fatigue life and damage are studied based on the experimental results. The fatigue life of the BRBs can be predicted using *Fatiga* and by inputting the strain history calculated from recorded displacements (output from LPs), that the BRB's core plate were subjected to under different test protocols. The rainflow counting method and Smith et al. (1970) method was used to calculate the damage caused by cycles at each stress-range amplitude. The total fatigue damage was accumulated by Miner's rule and is provided in Table 4. Because the BRB failed after applying these displacement histories, the total damage factor is also the calibration factor, which relates the base-metal low-cycle failure to that of a BRB, which will ultimately fracture because of repeated local buckling of the core plate. The calibration factor ranges from 0.0122 to 0.0486, with an average of 0.0363. For the BRB tested in the literature (Usami et al. 2011; Wang et al. 2012; Akira 2000; Maeda et al. 1998) using constant-amplitude strain loading, calibration factors ranging from 0.05 to 0.53 were reported. For strain ranges comparable with those reached during the BRB tests presented in this paper, these factors from previous experiments ranged from 0.05 to 0.11. The BRBs calibration factors obtained here are smaller than those reported in the literature. However, one must keep in mind that fatigue damage is dependent on the magnitude of the strain ranges and cycling sequence in the strain history, as well as on the type of BRB tested because different BRB detailing can lead to the development of different types of local buckling of the steel core.

Here, the reported calibration factors can be used to allow predicting the fatigue life of the BRB from a low-cycle fatigue perspective. However, more experimental works would be needed

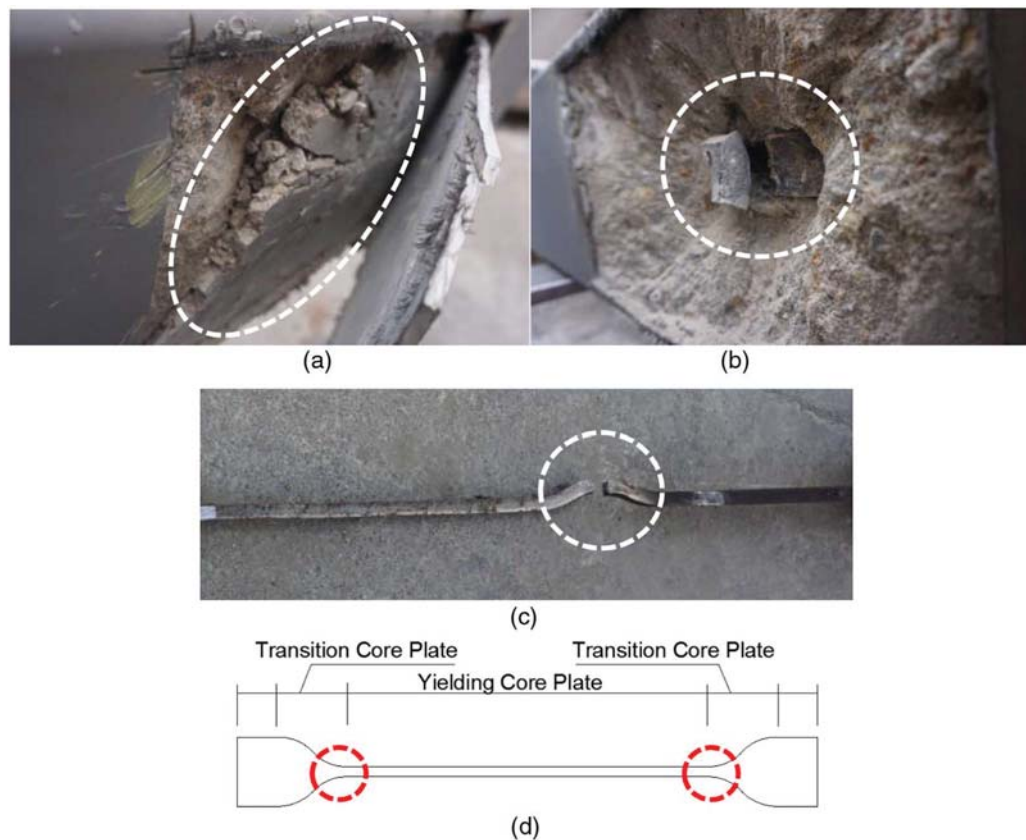


**Fig. 19.** BRB-2-4's failure observation: (a) concrete fractured around the broken core plate of BRB-2-4; (b) broken section of BRB-2-4's core plate; (c) core plate's fracture; (d) core plate buckling locations

**Table 3.** Summary of BRB's Cumulative Inelastic Deformations in Terms of Yield Displacement  $\Delta_{by}$

Specimen	Bidirectional	Axial	Total
BRB-2-1	$306\Delta_{by}$	0	$306\Delta_{by}$
BRB-2-2	0	$343\Delta_{by}$	$343\Delta_{by}$
BRB-2-3	$363\Delta_{by}$	$44\Delta_{by}$	$407\Delta_{by}$
BRB-2-4	$200\Delta_{by}$	$60\Delta_{by}$	$260\Delta_{by}$
BRB-1-1	$120\Delta_{by}$	$102\Delta_{by}$	$222\Delta_{by}$
BRB-1-2	$141\Delta_{by}$	$191\Delta_{by}$	$332\Delta_{by}$
BRB-1-3	$475\Delta_{by}$	0	$475\Delta_{by}$
BRB-1-4	$143\Delta_{by}$	$106\Delta_{by}$	$249\Delta_{by}$

**Table 4.** Summary of BRB's Fatigue Damage

Specimen	Bidirectional	Axial	Total damage
BRB-2-1	0.0122	0	0.0122
BRB-2-2	0	0.0486	0.0486
BRB-2-3	0.0225	0.0100	0.0325
BRB-2-4	0.0085	0.0050	0.0135
BRB-1-1	0.0097	0.0275	0.0372
BRB-1-2	0.0103	0.0248	0.0351
BRB-1-3	0.0416	0	0.0416
BRB-1-4	0.0104	0.0351	0.0455

to provide a statistical basis to generate generic predicting calibration factors for BRBs, based on the type of BRB specimen, as well as the magnitude and sequence of the applied strain history.

## Design Procedures

The following procedure is proposed to design bidirectional EDS for a given bridge at a known location. First, local displacement demands on the BRBs in bidirectional EDS should be obtained (Steps 1–6 as follows); the approach here is based on parametric analyses presented in Wei and Bruneau (2017):

1. Assume an initial value for the fundamental period of the EDS,  $T_{eff}$ . In this procedure, the EDS period is the same for the longitudinal and transverse direction. For a skew bridge, that would be the value for an equivalent nonskew EDS;
2. For the specified design acceleration response spectrum at the bridge location, which gives the elastic force demand of the bridge,  $mS_a$ , at its fundamental period,  $T_{eff}$ , choose a desired displacement ductility of the nonskew bridge EDS,  $\mu$ , the maximum of which can be taken as 6 per Eq. (4.3.3) in AASHTO (2011); calculate the corresponding force reduction factor,  $R$ , according to Eqs. (1) and (2)

$$R = \frac{\mu - 1}{\phi} + 1 \geq 1 \quad (1)$$

$$\phi = 1 + \frac{1}{12T_{eff} - \mu T_{eff}} - \frac{2}{5T_{eff}} \exp \left[ -2 \left( \ln T_{eff} - \frac{1}{5} \right)^2 \right] \quad (2)$$

3. The yield strength of nonskew EDS,  $V_y$ , is  $mS_a/R$ , the stiffness,  $K_{eff}$ , is  $4\pi^2m/T_{eff}^2$ , and the yield displacement of the EDS,  $\delta_y$ , is  $V_y/K_{eff}$ . The resulting inelastic displacement demand of the nonskew EDS is the elastic spectral displacement,  $\delta_y\mu$ , times the inelastic displacement magnification factor,  $R_{d1}$ , which is equal to 1.4;
4. Determine the displacement limits of the EDS: (1) the limit in the longitudinal directions,  $\delta_{Lm}$ , is the gap between the bridge

deck and abutment or the maximum seat width available; and (2) the limit in the transverse directions,  $\delta_{Tm}$ , is the girders' lateral yield displacement (for EDS with BRBs connected between girders), calculated based on the girder properties for a given steel bridge. Changes to the bridge design can be made to ensure that these two values are greater than the displacement demands calculated in Step 3. Alternatively, iterations over Steps 1–3 may be needed until the resulting displacement demands  $\delta_u$  in both directions are smaller than the limit;

5. For the bridge with skewness, the EDS is designed to have the same yield strength and displacement as its equivalent nonskew EDS designed following Steps 1–4. The displacement demand of the skew EDS,  $\delta_u$ , is calculated as  $\delta_{y\mu}R_{d1}R_{d2}$ , where  $R_{d2}$  is a displacement magnification factor relating the expected maximum displacement response of skew bridge to that of its equivalent nonskew bridge. For skew bridges with skew angles smaller than  $15^\circ$ ,  $R_{d2}$  could be taken as 1.1 and 1.3 for EDS-1 and EDS-2, respectively. For skew bridges with skew angles larger than  $30^\circ$ ,  $R_{d2}$  could be taken as 1.4 and 1.15 for EDS-1 and EDS-2, respectively [developments of these factors was presented by Wei and Bruneau (2017)]. For a skew angle beyond  $45^\circ$ , only the EDS-2 scheme is possible to satisfy the equal strength and displacement equivalent bridge assumption. Beyond  $60^\circ$  skew, the EDS-2 scheme would require BRB lengths that may not be practical; and
6. Determine the local displacement demand of the BRB based on the aforementioned displacement demand of the EDS,  $\delta_u$ .

Then design the BRB in the bidirectional EDS following either of the three approaches presented in the following Items (1)–(3) while satisfying the requirements in Items (4) and (5):

1. Implicit design: Select the minimum length of the longitudinal BRB's steel core to be at least 6% of the total length of the bridge (one longitudinal BRB at each end of the bridge). Based on the preceding findings (i.e., BRB having maximum cumulative inelastic deformations of 250 times the yield deformation as described in the "Cumulative Inelastic Displacements" section), this BRB can be left in service for 35 years and be expected to resist the seismic demand corresponding to the ductility of 6. This value can be modified to take into account the inclinations of the BRBs to reduce the length of the BRB yielding core as a percentage of total bridge length;
2. Explicit design: Select a longitudinal BRB yielding steel core length such that the sum of the cumulative ductilities corresponding to temperature-induced displacement demand and cyclic testing protocol does not exceed  $250\Delta_{by}$ . This may require iterations varying the length of BRB steel core, desired number of years in service, and expected BRB's ductility to resist the seismic demand;
3. Qualification testing (to be used if the preceding cumulative inelastic displacement limit of  $250\Delta_{by}$  is deemed too restrictive): BRB specimens can be qualified by subjecting one BRB to (1) the BRB standard test protocols (following AISC 341-10), followed by (2) the temperature-induced axial displacement history protocols applied repetitively for the number of years of service that the BRB is expected to provide in addition to the satisfactory seismic response; and a second identical BRB subjected to the same Protocols 1 and 2 but applied in the reverse order (i.e., Protocol 2 followed by Protocol 1). Qualification testing approach would be of benefit for BRBs of different fabrication/detailing (and possibly sizes) than those considered in this paper;
4. Determine the BRBs' end connections by (1) designing the end plates of the BRB to bend laterally to accommodate the required lateral displacement without developing instability; and

- (2) connecting the end plates of the BRB to a spherical bearing (special protection would be required to prevent corrosion of the spherical bearings); and
- Design the BRB connecting the gusset plate to resist 1.5 times the BRB yield strength. Limitations for the maximum gusset plate length and corresponding thickness are provided to ensure that the BRB can sustain the displacements demands without flexural yielding of the gusset plate connection.

## Conclusions

This paper has demonstrated the ability of BRBs implemented in bidirectional ductile end diaphragms to undergo bidirectional displacement demands while performing as intended. The BRB specimen with specifically designed end-connection details (either by having a long end plate or have the spherical bearing configuration) in the proposed bidirectional ductile EDS performed adequately through extensive cycles of inelastic deformations under both bidirectional and axial temperature-induced displacement test protocols. All BRB specimens failed in tension without end-plate failure or instability. A recommended design procedure was developed for designing the EDS in both skew and nonskew bridges based on these experimental results to ensure satisfactory BRB performance. Although the focus here was on implementation in bidirectional bridge ductile diaphragms, the findings on bidirectional behavior of BRBs can be valuable for other applications, given that bidirectional earthquake response is universal. As such, to further broaden applicability, testing of BRBs having greater strength or displacement capacity is certainly desirable and the logical next-step for future research, building on the findings presented in this paper.

## Acknowledgments

This study was sponsored by the Transportation Research Board of the National Academies under the TRB-IDEA Program (NCHRP-172). The authors acknowledge the oversight, valuable comments, and feedback from the NCHRP IDEA Project Advisor Lian Duan (California Department of Transportation) and other members of the Project's Expert Advisory Panel, namely Geoffrey Swett and Bijan Khalegi (Washington Department of Transportation), Taneja, Rajesh and Richard Marchione (New York Department of Transportation), Tom Ostrom (California Department of Transportation), and Phil Yen and Fred Faridazar (Federal Highway Administration). However, any opinions, findings, conclusions, and recommendations presented in this report are those of the authors and do not necessarily reflect the views of the sponsor.

## References

AASHTO. (2011). *AASHTO guide specifications for LRFD seismic bridge design*, 2nd Ed., Washington, DC.

AII (Architectural Institute of Japan). (2009). "Recommendations for stability design of steel structures." Tokyo 74–79.

Aiken, I. D., Mahin, S. A., and Uriz, P. (2002). "Large-scale testing of buckling-restrained braced frames." *Proc., Japan Passive Control Symp.*, Tokyo Institute of Technology, Tokyo, 35–44.

AISC. (2010). "Seismic provisions for structural steel buildings." *ANSI/AISC 341-10/341s1-10*, Chicago.

Akira, W. (2000). "Fatigue properties of practical-scale unbonded braces." *Nippon Steel Technical Rep. No. 82*, Nippon Steel, Tokyo.

Black, C. J., Makris, N., and Aiken, I. D. (2002). "Component testing, stability analysis and characterization of buckling restrained unbonded braces." *Technical Rep. PEER 2002/08*, Pacific Earthquake Engineering Research Center, Univ. of California, Berkeley, CA.

Bruneau, M., Uang, C. M., and Sabelli, R. (2011). *Ductile design of steel structures*, 2nd Ed., McGraw-Hill, New York, 921.

Celik, O., and Bruneau, M. (2007). "Seismic behavior of bidirectional-resistant ductile end diaphragms with unbonded braces in straight or skewed steel bridges." *Technical Rep. MCEER-07-0003*, MCEER, Univ. at Buffalo, Buffalo, NY.

Celik, O., and Bruneau, M. (2011). "Skewed slab-on-girder steel bridge superstructures with bidirectional ductile end diaphragms." *J. Bridge Eng.*, 10.1061/(ASCE)BE.1943-5592.0000141, 207–218.

Clark, P., Aiken, I., Kasai, K., and Kimura, I. (2000). "Large-scale testing of steel unbonded braces for energy dissipation." *Proc., Structural Congress*, ASCE, Reston, VA.

Fahnestock, L., Ricles, J., and Sause, R. (2007). "Experimental evaluation of a large-scale buckling-restrained braced frame." *J. Struct. Eng.*, 10.1061/(ASCE)0733-9445(2007)133:9(1205), 1205–1214.

*Fatiga version 1.03* [Computer software]. Fatec Engineering, Bergschenhoek, Netherlands.

FEMA. (2009). "Quantification of building seismic performance factors." *FEMA P-695*, Washington, DC.

Koetaka, Y., Kinoshita, T., Inoue, K., and Iltani, K. (2008). "Criteria of buckling-restrained braces to prevent out-of-plane buckling." *Proc., 14th World Conf. on Earthquake Engineering*, Beijing.

Lopez, W. A., Gwie, D., Saunders, M., and Lauck, T. (2002). "Lessons learned from large-scale tests of unbonded braced frame subassemblage." *Proc., 71st Annual Convention*, Structural Engineers Association, Sacramento, CA, 171–183.

López, W. A., and Sabelli, R. (2004). "Seismic design of buckling-restrained braced frames." *Steel Tips Rep.*, Structural Steel Educational Council, Moraga, CA.

Maeda, Y., Nakata, Y., Iwata, M., and Wada, A. (1998). "Fatigue properties of axial-yield type hysteresis dampers." *J. Struct. Constr. Eng.*, 63(503), 109–115.

Merritt, S., Uang, C. M., and Benzoni, G. (2003a). "Subassemblage testing of corebrace buckling-restrained braces." *Structural Systems Research Project Rep. No. TR-2003/01*, Univ. of California, San Diego.

Merritt, S., Uang, C. M., and Benzoni, G. (2003b). "Subassemblage testing of star seismic buckling-restrained braces." *Structural Systems Research Project Rep. No. TR-2003/04*, Univ. of California, San Diego.

Palmer, K., Roeder, C., Lehman, D., Okazaki, T., and Shield, C. (2013). "Experimental performance of steel braced frames subjected to bidirectional loading." *J. Struct. Eng.*, 10.1061/(ASCE)ST.1943-541X.0000624, 1274–1284.

Roeder, C. W., Lehman, D. E., and Christopoulos, A. (2006). "Seismic performance of special concentrically braced frames with buckling restrained braces." *Proc., 8th U.S. National Conf. on Earthquake Engineering*, Curran Associates, San Francisco.

Romero, P., Reaveley, L., Miller, P., and Okahashi, T. (2007). "Full scale testing of WC series buckling-restrained braces." *Final Rep. to Star Seismic*, Univ. of Utah, Salt Lake City.

Smith, K. N., Watson, P., and Topper, T. H. (1970). "A stress-strain function for the fatigue of metals." *J. Mater.*, 5(4), 767–778.

Takeuchi, T., Ozaki, H., Matsui, R., and Sutcu, F. (2014). "Out-of-plane stability of buckling-restrained braces including moment transfer capacity." *Earthquake Eng. Struct. Dyn.*, 43(6), 851–869.

Tremblay, R., Bolduc, P., Neville, R., and DeVall, R. (2006). "Seismic testing and performance of buckling-restrained bracing systems." *Can. J. Civ. Eng.*, 33(2), 183–198.

Tsai, K. C., et al. (2008). "Pseudo-dynamic tests of a full-scale CFT/BRB frame. I: Specimen design, experiment and analysis." *Earthquake Eng. Struct. Dyn.*, 37(7), 1081–1098.

Tsai, K. C., and Hsiao, P. C. (2008). "Pseudo-dynamic test of a full-scale CFT/BRB frame. II: Seismic performance of buckling restrained braces and connections." *Earthquake Eng. Struct. Dyn.*, 37(7), 1099–1115.

Tsai, K. C., Hsiao, B. C., Lai, J. W., Chen, C. H., Lin, M. L., and Weng, Y. T. (2003). "Pseudo dynamic experimental response of a full scale CFT/BRB composite frame." *Proc., Joint NCEE/JRC Workshop on Int. Collaboration on Earthquake Disaster Mitigation Research*, National Center for Research on Earthquake Engineering, Taipei, Taiwan.

- Uang, C. M., Nakashima, M., and Tsai, K. C. (2004). "Research and application of buckling-restrained braced frames." *Int. J. Steel Struct.*, 4, 301–313.
- Usami, T., Kasai, A., and Kato, M. (2003). "Behavior of buckling-restrained brace members." *Proc., 4th Int. Conf. on Behavior of Steel Structures in Seismic Areas*, Swets & Zeitlinger, Lisse, Netherlands, 211–216.
- Usami, T., Wang, C., and Funayama, J. (2011). "Low-cycle fatigue tests of a type of buckling restrained braces." *Procedia Eng.*, 14, 956–964.
- Wang, C. L., Usami, T., and Funayama, J. (2012). "Evaluating the influence of stoppers on the low-cycle fatigue properties of high-performance buckling-restrained braces." *Eng. Struct.*, 41(Aug), 167–176.
- Wei, X., and Bruneau, M. (2015). "Bidirectional-ductile end diaphragms for seismic performance and substructure protection." ([http://onlinepubs.trb.org/onlinepubs/IDEA/FinalReports/Highway/NCHRP172\\_Final\\_Report.pdf](http://onlinepubs.trb.org/onlinepubs/IDEA/FinalReports/Highway/NCHRP172_Final_Report.pdf)) (Nov. 2015).
- Wei, X., and Bruneau, M. (2016). "Buckling restrained braces applications for superstructure and substructure protection in bridges." *Technical Rep. MCEER-16-0009*, MCEER, Univ. at Buffalo, Buffalo, NY.
- Wei, X., and Bruneau, M. (2017). "Analytical investigation of buckling restrained braces' applications in bidirectional ductile end diaphragms for seismic performance of slab-on-girder bridge." *Eng. Struct.*, 141(Jun), 634–650.